

Do MLLMs Exhibit Human-like Perceptual Behaviors? HVSBench: A Benchmark for MLLM Alignment with Human Perceptual Behavior

Jiaying Lin^{*1,3}

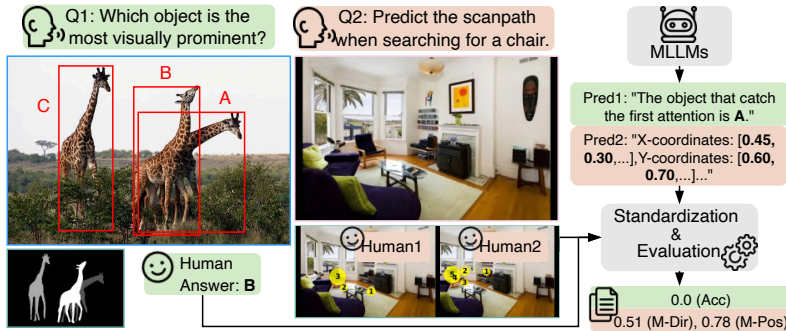
Shuquan Ye^{*2,3}

Dan Xu¹

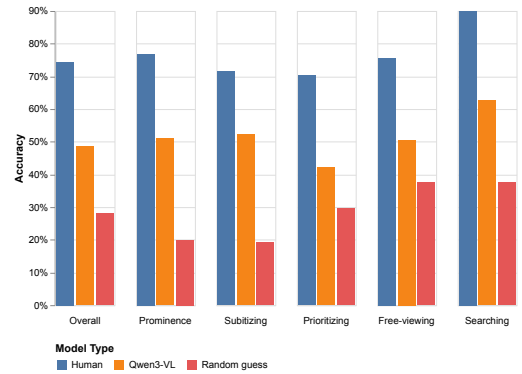
Wanli Ouyang²

Rynson W.H. Lau³

¹HKUST ²CUHK ³City University of Hong Kong



(a) HVSBench¹



(b) Results comparison.

Figure 1. We are the first to systematically study and assess MLLMs-HVS alignment. (a) We propose large-scale and comprehensive HVSBench, with a robust evaluation protocol. (b) Our comparisons among humans and the state-of-the-art model Qwen3-VL on HVSBench across 5 fields reveal room for improvement and insights for developing HVS-aligned MLLMs.

Abstract

While *Multimodal Large Language Models (MLLMs)* excel at many vision tasks, it is unknown if they exhibit human-like perceptual behaviors. To evaluate this, we introduce *HVSBench*, the first large-scale benchmark with over 85,000 samples designed to test MLLM alignment with the human visual system (HVS). The benchmark covers 13 categories across 5 key fields: Prominence, Subitizing, Prioritizing, Free-Viewing, and Searching. Our comprehensive evaluation reveals a significant perceptual gap: even state-of-the-art MLLMs achieve only moderate results. In contrast, human participants demonstrate strong performance, significantly outperforming all models. This underscores the high quality of HVSBench and the need for more human-aligned AI. We believe our benchmark will be a critical tool for developing the next generation of explainable MLLMs.

1. Introduction

Recent advancements in Multimodal Large Language Models (MLLMs) have shown remarkable progress, achieving impressive performance across diverse vision-language

tasks such as image captioning [6], visual question answering [17], mathematic reasoning [32], and more. Such achievements highlight the capabilities of MLLMs in perception and vision-language interaction.

Despite the impressive performance of MLLMs on vision tasks, we have limited understanding of why they perform well. It has been demonstrated in previous studies that principles inspired by the HVS and grounded in cognitive science [12], play a vital role in enhancing the performance of backbone models, such as attention-based architectures [46]. However, discrepancies remain in how MLLMs and humans perceive visual information. Human attention is based on innate and learned saliency, while MLLMs often perceive images as arrays of pixel values or feature embeddings. Human visual attention is sequential, adjusting based on context and prior knowledge, while MLLMs process input statically or through fixed-length attention. Human attention can be dynamically influenced and guided by goals, while MLLMs lack the cognition and the ability to “refocus” dynamically, relying purely on trained associations. Given the benefits and importance of HVS-aligned designs, including improving QA and captioning, content generation, downstream tasks, and practi-

^{*}Equal contributions. Project page: <https://jiaying.link/HVSBench/>

¹For brevity, only 2 of 10 human scanpaths are shown. Questions and predictions are simplified. Red overlaid boxes are NOT in original image.

cal applications, etc., as discussed in Sec. 4.4, the question of whether and to what extent existing MLLMs align with HVS remains a critical area for research, especially considering the current disparities.

This brings us to a fundamental question: *Do MLLMs perceive the world in the same way as humans do?* More specifically, *do MLLMs fixate on similar regions of interest within an image or follow a similar temporal order as the HVS when perceiving an image?* Humans can easily identify objects that capture their attention and perform visual searches based on context. However, in real-world scenarios, MLLMs often perceive visual information differently. For instance, in the first image of Fig. 1, if we ask, “Which object is the most visually prominent?”, most people would choose the center giraffe, while MLLMs identify the right one. Similarly, when searching for a chair in the second image, humans tend to first identify related objects (e.g., a table) and use contextual cues to help locate the chair (e.g., chairs are often near tables), while MLLMs may point to irrelevant areas. However, there has been limited research and challenges on how current MLLMs align with the HVS. On the one hand, existing public vision-language datasets are primarily designed to assess model performance on specific tasks, offering little insight into their alignment with HVS. On the other hand, traditional HVS research has largely focused on low-level, vision-only domains [34], often evaluating models based on masks or heatmaps, making it difficult to assess MLLMs where the primary output is text rather than visual data.

In response to these challenges, we introduce a comprehensive benchmark HVSBench and designed an evaluation protocol suite for MLLMs. Currently, HVSBench contains over 85K questions covering five distinct fields of the HVS, paired with images and answers:

1. **Prominence.** Test whether the regions MLLMs focus on align with those that are prominent to human perception. Example question in Q1 of Fig. 1.
2. **Subitizing.** Test whether the number of visually prominent objects for MLLMs matches human perception.
3. **Prioritizing.** Assess if the order of importance assigned by MLLMs to objects reflects human viewing priorities.
4. **Free-viewing.** Check if MLLMs can mirror the human attention shift (i.e., sequence of locations that the HVS attends to) in an image during free viewing.
5. **Searching.** Test if MLLMs can follow a similar sequence of gazes as humans when searching for a specific object in an image. Example in Q2 of Fig. 1.

The questions can be categorized into 13 types based on their phrasing, and the answer types include multiple-choice, counting (i.e., predicting an integer value), sorting, and scanpath prediction. To ensure both quality and variability, we design our benchmark based on a curated collection of large-scale and high-quality datasets [7, 11, 34, 49]

focusing on the HVS derived from real-world human studies. For a balanced assessment of each field, we carefully curate and divide the question field so that each field encompasses over 6,707 questions. For the evaluation protocol, while pure exact-match metrics are unreliable due to the limitations of MLLMs in instruction-following and choice labeling, GPT-4-based matching adds bias, costs, and struggles with complex predictions like scanpaths. Thus, to reduce the matching-caused false-negative and improve evaluation robustness across fields, we design a human-inspired and field-adaptive automatic standardization, taking inspiration from diverse possible predictions.

We thoroughly evaluate 26 well-known SOTA MLLMs and human performance on HVSBench, spanning diverse architectures and model scales. This not only provides a direct comparison among these models across multiple aspects of the HVS, but also highlights the significant gap between current MLLMs and humans. Furthermore, our findings reveal critical insights for future improvements: aligning MLLMs with the HVS cannot be achieved merely by incorporating external knowledge of related cues and priors, or by integrating human-generated captions and summaries. Additionally, we stress the value of HVS alignment across domains and their evidences: mimicking human fixation enhances QA/captioning; more intuitive content generation demonstrated by our designed prominence enhancement; improved performance in HVS-specific tasks; and applications in autonomous driving and assistive tools. Our contributions are summarized as follows:

1. To the best of our knowledge, we are **the first** to systematically study the perceptual alignment between MLLM and the HVS, across five distinct fields of HVS for model evaluation.
2. We construct HVSBench, **the first** large-scale and comprehensive benchmark with 85,147 multimodal question-answer pairs to thoroughly evaluate MLLMs in scenarios that closely mirror the HVS.
3. We propose a robust evaluation protocol with a human-inspired and field-adaptive automatic standardization.
4. We conduct a comprehensive evaluation of 26 popular MLLMs and human using HVSBench. Additionally, we provide new insights and techniques for developing more HVS-aligned and explainable MLLMs.

2. Related Work

Existing benchmarks for MLLMs focus on assessing their capabilities in understanding and reasoning across modalities. A wide range of benchmarks, such as MMBench [30] and SEEDBench [25], evaluates general multimodal capabilities, including visual perception, reasoning, and comprehension. These benchmarks span diverse tasks, including document understanding [35], visual question answering [33], hallucination detection [28] and mathematical rea-

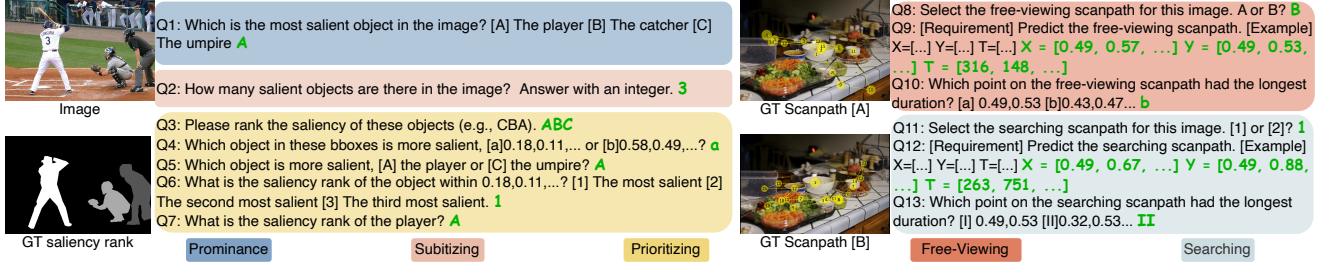


Figure 2. Simplified Samples of 13 question types in HVS Bench. GT ranks and scanpath plots are for better visuals.

soning [32]. While existing benchmarks assess various abilities, they do not fully evaluate the alignment of MLLMs with the HVS. The introduction of HVS Bench addresses this gap, focusing on human-centric evaluation to reveal the secret of how MLLMs perceive and process visual information. More related work on different areas is in the supplementary material.

3. HVS Bench

We define the five distinct fields of HVS, followed by a description of multimodal QA generation, and automatic standardization and evaluation protocol. Fig. 2 shows some examples in our HVS Bench. The Sec. 1 and Sec. 4 in supplementary materials provide the rationale behind selecting fields, their corresponding source datasets, additional samples and the results for each question type.

3.1. Preliminaries

To evaluate MLLM alignment with the HVS, we construct multimodal QAs based on five key fields, selected to represent diverse aspects of human visual processing and provide a comprehensive assessment. They include:

- **Prominence.** Identifying the most visually salient objects in a scene, reflecting human visual focus.
- **Subitizing.** Rapidly estimating the number of salient objects, requiring parallel attention and useful for tasks like crowd analysis.
- **Prioritizing.** Ranking objects by perceptual saliency to capture dynamic visual importance, with applications in explainable decision-making.
- **Free-Viewing.** Modeling bottom-up gaze patterns in task-free settings with insights into visual attention.
- **Searching.** Capturing top-down gaze behavior during goal-driven tasks, influenced by semantic context, supporting efficient, adaptive attention.

The selection of the five key fields is grounded in the dual-process theory introduced in [3], which distinguishes between bottom-up (stimulus-driven) and top-down (goal-directed) processes. Bottom-up processes mainly include prominence [18], free-viewing [19] and subitizing [45]. Top-down processes mainly include prioritizing [15] and

searching [14]. These fields were chosen because they span the majority of human visual behavior, as shown in reviews on visual scene processing [16], which emphasizes saliency (Prominence), attention dynamics (Free-Viewing), and search (Searching) as critical components of HVS. While others may exist, these five fields are the most widely studied and theoretically validated in HVS to the best of our knowledge.

3.2. Benchmark Curation

Based on the above definitions, we design an automatic multimodal QA generation paradigm to convert source annotations into different forms of QAs for MLLM evaluation. **Multimodal QA Generation.** Since the annotations in the selected datasets are not in the multiple-choice QA format, we automatically transform the ground-truth annotations into this format automatically with human verification. Specifically, we manually created 13 types of question templates. Following previous practices [30], most of our evaluations are conducted using multiple-choice QAs rather than open-ended ones, except for fields with well-defined outputs such as reporting a positive integer (e.g., subitizing) or a list of coordinates (e.g., scanpath prediction). These formats align directly with their problem metrics, enabling precise and unbiased evaluation. Open-ended answers often require scoring by LLMs or user studies, which can introduce evaluation bias or require manual intervention based on previous practices [30]. Then, we create the corresponding answer options as follows.

Variations in perception. We leverage **GT human** data in peer-reviewed cognitive science datasets [7, 11, 34, 49] rigorously designed for diversity and bias control. For example, Fig. 1’s source [11] employs 8 annotators (a common sample size [27] in saliency research) in diverse culture (EU/CN), race (Black/White/Asian), and gender (4M/4F), collected by strict protocols (e.g., eye-tracking monitor) to minimize bias. This ensures our benchmark captures shared human attention tendencies, aligning with common practices in HVS research.

(1) Template-Based Construction: For most questions, we generate answer options directly from GT human annotations. For example, in fields like **Prominence**, the op-

tions are derived from bounding boxes or other directly annotated features. To ensure diversity in the questions, we design multiple templates for **each** question type, following the methodology outlined in [29]. These templates provide variation while maintaining the focus of the field. For instance, in Prominence, we use templates such as:

- Which object is the most salient in the image?
- Which object is the most visually prominent?
- Which object attracts the highest visual attention?

All templates are manually created by humans to ensure accuracy and relevance.

(2) LLM-Based Refinement: Note that some MLLMs may not be able to utilize the coordinate data well, but they are more suitable for interpreting in natural language. We design a bunch of questions that do not explicitly involve numerical data. However, such data cannot be easily obtained due to the limited original label types of data sources. For scenarios where bounding box coordinates are not explicitly required and the field involves natural language references (e.g., *Between these two objects — [A] <obj1> [B] <obj2> — please select the option representing the more salient object.*), we use a large language model (LLM) [1] to generate description in natural language for the options ([A] **the person on the left side**; [B] **the bicycle on the right side**). Specifically, we use GPT-4 [1] to describe objects based on their bounding boxes and to create plausible but false options from non-salient objects. This method ensures that the QA matches real-world applications where natural language complements visual data.

(3) Human verification. To address potential ambiguities introduced by LLMs or the complexity of image content in (2), human verification is employed to ensure that the referred objects in natural language descriptions correspond accurately to the intended targets. This additional step improves the accuracy and reliability of generated QAs.

Answer Option Processing. For multiple-choice questions, we randomly sample answer options from the available candidates and shuffle their order. This approach enhances robustness by minimizing biases arising from fixed option orders or repetitive patterns in the answer choices. For scanpath-related questions (i.e., free-viewing and searching), following [49], we randomly sample human scanpaths from different images. This ensures that the alternative answer options are also derived from human data, making them more natural. By avoiding reliance on computer-generated scanpaths, we ensure that the evaluation remains unbiased and fair for the evaluated LLMs.

To this end, we produced 85K multimodal QAs based on annotations from 71K images, covering 13 question types across 5 key fields in HVS, including prominence, subitizing, prioritizing, free-viewing and searching. Table 1 shows statistics of our HVSBench, which is large and diverse, covering various answer types and tasks.

	Prominence Q1	Subitizing Q2	Prioritizing Q3-Q7	Free-Viewing Q8-Q10	Searching Q11-Q13
Total QAs	8,389 (11%)	18,105 (24%)	26,309 (34%)	17,090 (22%)	6,707 (8%)
85,147	Question Categories	Average # of Obj.	Max./Avg. Q Length	Max./Avg. A Length	Max./Avg. # of Choice
	13	3.2	104/45.8	5/1.4	17/3.9

Table 1. Key statistics of HVSBench. Fixation prediction statistics are excluded due to lengthy answers.

3.3. Automatic Standardization and Evaluation

Automatic Standardization. In evaluation protocols, pure exact-match metrics prove unreliable due to the limitations of MLLMs in instruction-following. For example, in Fig. 3, even when we explicitly specify the output format and provide example outputs for reference, MLLMs still produce predictions with inconsistent and somewhat random formatting. Meanwhile, the widely adopted LLM-based matching approaches [13] introduce biases, incur high costs due to multiple evaluation passes, and struggle with complex predictions such as scanpaths. To address these challenges, we propose a human-inspired, field-adaptive automatic standardization method. It minimizes false negatives caused by matching errors and enhances evaluation robustness by programmatically adapting to diverse prediction formats across the five fields in our benchmark.

To achieve automatic standardization programmatically, we adopted a human-inspired, field-adaptive approach. Specifically, we observed that the responses to each question type are not open-ended but instead follow discernible patterns. Building on this insight, for each field, we randomly sampled 10 example questions for each question type. On these example questions, we then collected multiple rounds of random predictions from all models evaluated in our experiments, as well as predictions from over 20 different human participants and their human-annotated standardizations. With these diverse and complex predictions across fields, we programmatically defined an automated standardization process. This process ensures robust performance without errors, even on unseen predictions.

For the **Prominence** field, the automatic standardization cleans and normalizes predictions into consistent main choice labels (e.g., ‘A’, ‘C’, etc.) from various input formats, using regex to detect explicit or implied labels in diverse phrasing. For **Subitizing**, the automatic standardization processes predictions to extract integer values, including direct numbers, text-based numbers (e.g., “three”), or implied quantities. When no valid number is found, it defaults to the average ground truth value in 3.2116. For **Prioritizing**, except for choice answers that are processed the same as in the Prominence field, our automatic standardization detects and normalizes answers of sequence (sorting) via order-related phrasing through regex patterns. In **Free-viewing** and **Searching** fields, The automatic standardization involves extracting and normalizing scanpath data (X,

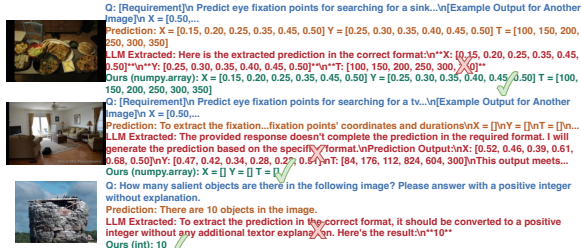


Figure 3. Illustration of our automatic standardization, which robustly formats predictions without introducing errors. In contrast, LLM-based matching (e.g., GPT-4) is both costly and prone to errors, such as failing to extract the correct format or predicting unrelated outputs.

Y for coordinates and T for durations) from diverse input formats, including text, JSON, and various phrasing styles. It also addresses irregularities like mismatched list lengths and incomplete scanpaths. Refer to Sec. 2 in supplementary for predictions and their corresponding standardized outputs in each field. We illustrate the superiority of our automatic standardization over LLM-based matching in Fig. 3. In our experiments, GPT-4 was prompted with the full question, the full prediction, and the text prompt: “Please extract the prediction with the correct format.” Refer to Sec. 3 in supplementary for detailed inputs, experimental settings, and pseudo-code for our automatic standardization.

Evaluation Metrics. In the **Prominence** field, we use accuracy in which are choice questions. For the **Subitizing** field, we adopt widely used metrics, including Mean Absolute Error (MAE), Root Mean Square Error (RMSE), as well as Exact Match Accuracy (Acc). For **Prioritizing**, the answer types include single-choice and sequence (sorting). The single choices are evaluated via accuracy. To evaluate whether the predicted order matches the ground truth exactly, Exact Match Accuracy (Acc) is also used. In **Free-viewing** and **Searching**, we employ the widely adaptive MultiMatch [19] similarity to evaluate generated scanpaths across shape, direction, length, and position. Our main results focus on the direction (“M-Dir”) and position (“M-Pos”) for simplicity. Following standard procedures [49], predictions are cropped to length 6, with final scores for each prediction being MultiMatch averaged over 10 GT scanpaths in the image.

4. Experiments

4.1. Evaluation Details

In Subitizing of random guess, accuracy is computed using random sampling based on the frequency distribution of subitized object counts. Our human evaluation involves 10 participants from diverse backgrounds, considering individual differences [21]. For MultiMatch, we use a commonly used oracle method [49], which com-

pares each subject’s scanpath as a prediction to others’ as GT and averages the results. We select recent

open-source MLLMs for validation, including DeepSeek-VL [31], Idefics-series [23, 24] LLaVA-Next [29], LLaVA-OneVision (LLaVA-OV) [26], mPLUG-Owl3 [53], Qwen-VL series [47], InternVL-series [8], ERNIE-4.5-VL [38], MiniCPM-V 2.6 [52] and GLM-4V series [41]. We evaluate a range of model scales, from 7B up to 235B. Note that we still focus on 7B-scale models for both efficiency, effectiveness and fair comparisons among baselines by selecting most baselines at this scale. We also include GPT series [1] and Gemini series [39], two representative proprietary MLLMs, as baselines in our evaluation. All experiments are conducted using VLMEvalKit [13] on the same platform for consistency and fairness. We allocate 10% of HVSbench for evaluation and reserve the remaining 90% for further explorations such as instruction-tuning MLLMs.

4.2. Main Results on HVSbench

Quantitative Evaluation. Table 2 presents the evaluation results on HVSbench, highlighting that current open-source and proprietary MLLMs still underperform in aligning with HVS. Diverse human participants achieved strong performance (OA: 0.7438). Given individual differences in saliency and cognitive science [21], this performance is both high and reasonable, which further validates the quality of our benchmark. Humans (OA: 0.7438) clearly outperform both random guessing (OA: 0.2806) and the best MLLMs (best OA: 0.4851) in all metrics. The top-performing MLLMs are the open-source Qwen3-VL-235B (OA: 0.4851) and the proprietary Gemini-2.5-pro (OA: 0.4754). Notably, the best open-source model slightly outperforms the best proprietary model. Both models significantly surpass older models like GPT4-o (OA: 0.3946), demonstrating the rapid potential of recent MLLMs.

In Free-viewing (Acc Q8,Q10), several models now outperform random guessing (0.3750), including LLaVA-OneVision (0.3888), Gemini-2.5-pro (0.4082), and the top-performing Qwen3-VL-235B (0.5054). The performance is even stronger in Searching (Acc Q11,Q13), where numerous models like LLaVA-OneVision (0.4913), Gemini-2.5-pro (0.5810), and Qwen3-VL-235B (0.6259) significantly surpass the random guess baseline (0.3752). A possible explanation is that in Free-viewing, which is a pure vision field that reflects HVS behavior without conditioning, these models exhibit behaviors that differ from humans. In contrast, Searching involves more defined objectives and patterns that are uniform and predictable, making them easier for MLLMs to align with.

Despite this progress, the gap to human performance remains. These results suggest significant room for scanpath prediction for current MLLMs. The Sec. 6 in supplementary materials shows the detailed benchmark on all 13 ques-

Models	Overall Acc \uparrow	Prominence		Subitizing		Prioritizing	Free-viewing			Searching		
		Q1 Acc \uparrow	Q2 Acc \uparrow	Q2 MAE \downarrow	Q2 RMSE \downarrow	Q3-Q7 Acc \uparrow	Q8,Q10 Acc \uparrow	Q9 M-Dir \uparrow	Q9 M-Pos \uparrow	Q11,Q13 Acc \uparrow	Q12 M-Dir \uparrow	Q12 M-Pos \uparrow
Human Performance												
Human	0.7438	0.7683	0.7143	0.6349	1.3333	0.7025	0.7560	0.6963	0.8863	0.9000	0.7617	0.9181
Baselines												
Random guess	0.2806	0.1994	0.1909	-	-	0.2949	0.3750	-	-	0.3752	-	-
Proprietary MLLMs												
GPT4-o	0.3946	0.3139	0.4512	1.3445	3.2614	0.3621	0.3737	0.5917	0.8042	0.4015	0.5106	0.7834
GPT5-nano	0.4435	0.4664	0.4931	1.1840	2.2897	0.4117	0.3939	0.5961	0.8143	0.5885	0.4884	0.8004
GPT5-mini	0.4675	0.4896	0.5493	1.0080	2.0429	0.4219	0.3969	0.6088	0.8100	0.6509	0.6150	0.8394
Gemini-1.5-Flash	0.3886	0.3323	0.5106	1.3070	3.0978	0.3283	0.3804	0.6128	0.8392	0.4040	0.5199	0.8206
Gemini-2.0-flash	0.4049	0.4652	0.4602	1.9602	23.3327	0.3839	0.3588	0.5739	0.8239	0.3616	0.4876	0.8358
Gemini-2.0-flash-lite	0.3556	0.3932	0.3208	2.0530	4.4785	0.3495	0.3778	0.6085	0.7996	0.3915	0.5411	0.8170
Gemini-2.5-flash	0.4221	0.4408	0.3865	2.2709	5.9720	0.4215	0.4142	0.6298	0.8393	0.5885	0.6252	0.8540
Gemini-2.5-flash-no-thinking	0.4148	0.4774	0.4321	2.0069	4.9635	0.4061	0.3778	0.6165	0.8481	0.4214	0.5221	0.8202
Gemini-2.5-flash-lite	0.4071	0.4457	0.4608	1.3977	4.1724	0.3720	0.3915	0.5640	0.8460	0.3840	0.4693	0.8361
Gemini-2.5-pro	0.4754	0.5189	0.5308	1.1501	2.5422	0.4505	0.4082	0.6251	0.8396	0.5810	0.6378	0.8583
OpenSource MLLMs												
DeepSeek-VL	0.3655	0.3223	0.4544	1.2471	2.2514	0.3327	0.3445	0.5118	0.5450	0.3516	0.4790	0.7130
Idefics2	0.3067	0.2015	0.2990	2.2078	3.8573	0.2971	0.3637	0.5151	0.5525	0.3865	0.5322	0.7619
Idefics3	0.3552	0.2149	0.4852	1.1055	1.9567	0.3272	0.3411	0.5329	0.6310	0.2843	0.5407	0.6856
LLaVA-Next	0.3460	0.3223	0.3961	1.3727	2.2675	0.3341	0.3274	0.5249	0.5998	0.3192	0.5083	0.7883
LLaVA-OneVision	0.4035	0.4640	0.4517	1.1206	1.9671	0.3495	0.3888	0.5490	0.8177	0.4913	0.5047	0.7295
mPLUG-Owl3	0.3076	0.3309	0.2688	2.8941	4.6162	0.3305	0.3117	0.5028	0.4941	0.2668	0.5368	0.5592
MiniCPM-V 2.6	0.3476	0.3748	0.4491	1.2471	2.1137	0.2989	0.3023	0.5132	0.5589	0.3416	0.4953	0.7107
ERNIE-4.5-VL-28B-A3B	0.3936	0.4115	0.4496	1.5673	3.7682	0.3599	0.3766	0.5562	0.8495	0.3990	0.5120	0.7913
InternVL2.0	0.3082	0.3101	0.3405	2.3458	3.6068	0.3405	0.3409	0.5028	0.7090	0.2968	0.5016	0.7282
InternVL3.5-8B	0.4254	0.4811	0.5111	1.1426	2.1146	0.3839	0.3564	0.5013	0.6447	0.4863	0.4683	0.7919
GLM-4.1V-9B-Base	0.3932	0.4664	0.4040	1.3828	2.3392	0.3961	0.3474	0.5139	0.7772	0.3641	0.4976	0.7625
GLM-4.1V-9B-Thinking	0.4191	0.4872	0.3834	1.9067	3.6251	0.4057	0.4195	0.6022	0.7902	0.5387	0.5113	0.8351
GLM-4.5V	0.4640	0.4737	0.5286	1.2582	2.6779	0.4380	0.3999	0.5982	0.7756	0.5885	0.5343	0.8096
Qwen2-VL-7B	0.4076	0.4103	0.5090	1.4698	2.6747	0.3901	0.3182	0.5199	0.7178	0.4214	0.4610	0.8200
Qwen3-VL-8B	0.4320	0.4811	0.4539	1.1363	1.9546	0.4090	0.4011	0.5122	0.8421	0.5187	0.4812	0.8613
Qwen3-VL-235B-A22B	0.4851	0.5092	0.5223	1.0483	1.9148	0.4204	0.5054	0.5665	0.8468	0.6259	0.5109	0.8517

Table 2. **HVSBench Leaderboard.** The results of MLLMs reveal significant room for improvement.

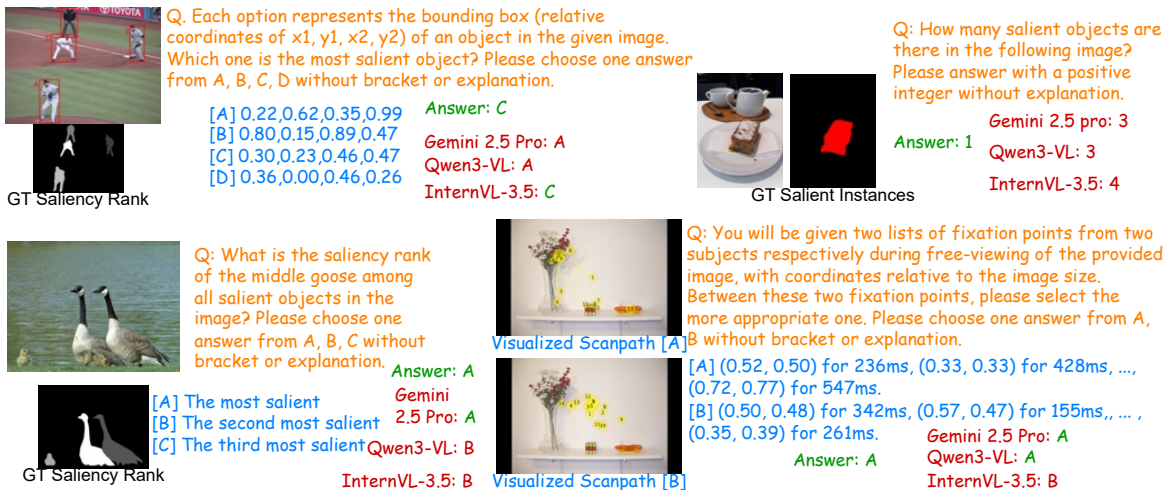


Figure 4. Qualitative results. The bounding boxes, the scanpaths and the GT masks from the source datasets (e.g., rank & instances) are for visual clarity and not used in the input images for evaluation. Text is partially omitted due to limited space.

tion types.

Benchmark Examples and Predictions. Fig. 4 shows examples and results of the three best-performed and representative models. We include the GT saliency information based on natural viewing by human observers for reference. The top-left illustrates a sample from the Prominence field.

A human can easily identify the person closest to the center as the most salient. However, both Gemini 2.5 Pro and Qwen3 fail in this case. The top-right corner shows a sample from the Subitizing field. All baselines fail to predict the correct quantity. The bottom-left corner features a sample from the Prioritizing field, where only Gemini 2.5 Pro

succeeds. The bottom-right corner displays a sample from the Free-Viewing field. Option A reflects a clear pattern of human attention, while the human scanpath shown in option B is unrelated to the image. Despite this, the InternVL-3.5 incorrectly selected B. The bottom-right shows a surprising case in our HVS Bench where advanced MLLMs can select the human free-viewing scanpath correctly, even though such a task is purely vision and not included in their training objectives. This highlights that the advanced MLLMs behavior in purely vision tasks may have some similar properties like those in HVS. Refer to Sec. 4 in the supplementary for more qualitative results.

Do thinking models outperform non-thinking models? Recent MLLMs show outperformance by utilizing thinking processes. To investigate this, we manually disable the thinking process of gemini-2.5-flash (“gemini-2.5-flash-no-thinking”) and found that its non-thinking model generally performs worse than the origin thinking model. In particular, the overall accuracy drops from 0.4221 to 0.4148, while we observe a significant drop in the searching section (Acc: 0.5885→0.4214). This is reasonable since visual search requires contextual modeling during its searching process and a thinking-based model is good at it.

MLLMs’ Explanation on its Choice. Taking the bottom left image used in Fig. 4 as an example, Gemini 2.5 Pro can explain why it predicts the middle goose is the most salient: *Size: It is a large subject in the image. Contrast: Its long, black neck and distinct white cheek patches create a strong visual contrast against its own body and the muted green water in the background. Position: It is centrally located and in sharp focus, acting as the primary focal point of the image.* This explanation shares the findings from cognitive science on HVS [18], and it shows advanced MLLMs like Gemini 2.5 Pro can somehow align with HVS and understand the concept of saliency.

MLLMs’ Scanpaths v.s. Human’s GT. In Fig. 5 shows that the GT scanpaths obtaining from humans focus on text and informative areas, while MLLMs’ scanpaths are generally reasonable (focus on objects), slightly differing from humans (text first). This shows MLLMs share similar observing pattern with humans but still have a significant gap, as shown in Table 2.

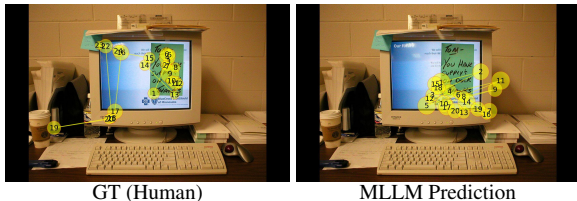


Figure 5. MLLMs’ predictions differ from GT reasonably. MLLMs and GT differ clearly from random guess.

Baselines	# Param	PO↑	SU↑	PI↑	FV↑	SE↑
GPT4-o mini	N/A	0.3126	0.4480	0.3312	0.3560	0.3766
GPT4-o	N/A	0.3139	0.4512	0.3621	0.3737	0.4015
DeepSeek-VL	1.3B	0.1758	0.2513	0.2950	0.3188	0.2843
	7B	0.3223	0.4544	0.3327	0.3445	0.3516

Table 3. **Ablation study of the number of params.** PO, SU, PI, FV and SE means “Prominence”, “Subitizing”, “Prioritizing”, “Free-viewing”, “Searching”, respectively.

4.3. Ablation Study

Model Size. We assess model size impact on HVS Bench by testing models with different parameter counts. We select two representative methods: DeepSeek-VL [31] and GPT-4o [1], from both open-source and proprietary MLLMs, for comprehensive analysis. As shown in Table 3, larger MLLMs generally outperform smaller ones across all metrics. It suggests that increasing model size leads to better alignment with HVS for MLLMs. Refer to the supplementary for more experiments.

Human Captions or Descriptions Improve Alignment?

It is possible that certain annotations, like human captions from COCO caption and detailed descriptions from LLaVA-Instruct-150K, implicitly reflect the HVS. Therefore, we evaluated whether adding detailed descriptions (“Detail.”) or short captions (“Cap.”) could improve the performance of the base GPT-4o model. As shown in Table 4, in the field of Prominence and Subitizing, adding detailed descriptions and captions improved performance, suggesting that additional information helps the model better identify and subitize visually dominant elements. In Prioritizing, while detailed descriptions provided some improvements, captioned input worsened the score, suggesting that brief caption information may not be sufficient for understanding object importance in a human-aligned way. In Free-viewing, both detailed descriptions and captions actually lowered performance. These results suggest that neither detailed descriptions nor captions can effectively capture human attention shifts in free-viewing. In Searching, captions slightly improve accuracy, while detailed descriptions reduce accuracy.

One reason may be that humans typically shift their attention rapidly between the most salient objects when searching. Captions, by prioritizing only the most salient features, better mirror this fast-paced, targeted attention. Detailed descriptions, however, broaden the focus range, leading to attention that doesn’t align with human searching. These results suggest that providing more context through human captions or detailed descriptions can lead to better performance in some evaluation criteria, aligning MLLMs with the HVS cannot be achieved merely by integrating human-generated captions and summaries, especially in Prioritizing, Free-viewing and Searching fields.

Field-Specific Hints Improve Alignment? Since definitions and prior knowledge of the fields also provide cues for

Baselines	Hint	PO \uparrow	SU \uparrow	PI \uparrow	FV \uparrow	SE \uparrow
	\times	0.3139	0.4512	0.3621	0.3737	0.4015
GPT-4o	Detail.	0.4274	0.4809	0.3799	0.3465	0.3791
	Cap.	0.4188	0.4852	0.3464	0.3605	0.4190

Table 4. Ablation study of question prompt.

Baselines	Task	PO \uparrow	SU \uparrow	PI \uparrow	FV \uparrow	SE \uparrow
	\times	0.3139	0.4512	0.3621	0.3737	0.4015
GPT-4o	\checkmark	0.4212	0.5005	0.3803	0.3476	0.3342

Table 5. Ablation study of system prompt.

Baselines	Search Length \downarrow
Random-DFS	9.97
Human Fixation	2.52

Table 6. Human fixation can guide the visual search process in [48] on COCO-Search18, obtaining from [48] with simplification.

the HVS, we examine whether adding Field-Specific Hints can enhance model performance. For example, the simplified hint for the Prominence field is: *The detection of salient objects aims to simulate the human visual perception system by identifying and localizing the most visually striking object(s) in a scene. ... (omitted), cues such as color contrast, spatial bias, and depth contrast also influence saliency. Refer to Sec. 5 in supplementary for full hints in each field.*

Table 5 summarizes the results on GPT-4o. Our results show an improvement in the Prominence, Subitizing, and Prioritizing fields but a noticeable decrease in performance for Free-viewing and Searching. This decline suggests that too much contextual information may hinder the model’s focus on the raw visual features necessary for free-viewing tasks. A possible explanation is that prior knowledge might cause the model to focus immediately on specific parts of the image, disrupting the natural temporal sequence of the human gaze. This could lead to fixation sequences that are less representative of human free-viewing or searching.

4.4. Discussion: Benefits and Applications

While human perception mimicry may not be universally beneficial, but we stress its value in key tasks. (1) Mimicking human perception can significantly improve tasks requiring precise visual grounding, such as QA, captioning and visual searching. As shown in Table 6 (which is obtained from the Table 4 of [48]), models mimicking human fixation mechanisms achieve shorter search lengths on COCO-Search18, improving efficiency and accuracy. (2) In HVS-related downstream tasks, models better aligned with HVS perform better. For example, Qwen2-VL outperforms MiniCPM-V in our HVS-Bench and also in general tasks such as human perception, visual illusion (MMM-U, HallucinationBench), but is comparable or worse in tasks unrelated to HVS like math reasoning (MathVision). (3) Practical applications like autonomous driving, perception in robots, assistive tools for the visually impaired, and tasks directly related to the HVS (e.g., saliency prediction), further demon-



Figure 6. Application: Smart Thumbnailing. Based on the results from Table 5 (PO: w/o task definition 0.3139 \rightarrow w/ task definition 0.4274), GPT-4o with better performance on prominence (i.e., w/ task definition, PO: 0.4274) can generate a better smart thumbnail than the one w/o task definition (PO: 0.3139).

strate the benefits where HVS alignment ensures intuitive, user-centered outputs. (4) We also provide a potential application and show that content generation models better aligned with the HVS can produce more reasonable outputs. Taking the prominent field as an example, we design a smart thumbnailing based on cropping and prominence enhancement to illustrate as shown in Fig. 9. Specifically, we examine how GPT-4o crops the image to enhance the prominence of one object: a photo. GPT-4o with a task-specific hint generates a reasonable analysis and successfully crops the image to highlight the photo, compared to the result without hint, demonstrating better alignment with HVS. This can be directly applied to automated design, context-aware content generation, and visual storytelling.

Based on these aspects, we believe mimicking human perception will benefit machine vision.

5. Conclusion

In this paper, we explore the alignment between MLLMs and the human visual system. We introduce HVS-Bench, a novel large-scale benchmark designed to evaluate MLLMs on vision tasks that closely mirror human perception. It consists of 85K multimodal QAs across 13 categories and 5 fields, accompanied by a robust evaluation protocol. Our experiments demonstrate that HVS-Bench poses a new, significant challenge for state-of-the-art MLLMs, highlighting considerable room for improvement. We believe HVS-Bench will drive the development of more human-aligned and explainable MLLMs, offering critical insights into how these models perceive and process visual information.

Do MLLMs Exhibit Human-like Perceptual Behaviors? HVSBench: A Benchmark for MLLM Alignment with Human Perceptual Behavior

Supplementary Material

The supplementary materials include:

- Section 1: Preliminary Settings for HVBench**

This section explains the rationale behind the selection of fields for HVBench. It also provides details about the corresponding source datasets used for each selected field.
- Section 2: Sample Prediction and Standardization**

We present the predictions generated by the models and the corresponding outputs after applying our standardization process for each field. This ensures consistency and comparability across different fields.
- Section 3: Detailed Settings**

This section provides detailed settings in our experiments and standardization pipeline, including the inputs used in our experiments, the detailed experimental settings, and the pseudo-code for our automated standardization pipeline.
- Section 4: Additional Qualitative Examples and Results**

We include extra qualitative examples showcasing sample questions and the predictions made by MLLMs under each field.
- Section 5: Field-Specific Hints in Each Field**

For each field, we provide specific hints or context that help understand tasks.
- Section 6: Detailed Benchmark Results and Discussions**

This section contains a detailed report of benchmark results for all 13 question types, offering a comprehensive view of the performance across various fields and question types. We also provide additional ablation studies and related discussions for them.
- Section 7: More Related Work**

We include more related work for different research areas to showcase the necessity of our HVSBench.
- Section 8: Application:**

We include an application, which shows that content generation models better aligned with the HVS can produce more reasonable outputs.

6. Preliminary setting for HVBench

To evaluate the extent to which multimodal large language models (MLLMs) align with the HVS, we construct multimodal queries based on five fields designed for different datasets. These fields are critical for assessing whether MLLMs perceive and interpret visual information in a manner akin to humans. For a fair and comprehensive evalua-

tion, the five fields are carefully curated to capture different aspects of the HVS. These fields include:

Prominence. The prominence in HVS enables humans to identify the most visually prominent objects within an image [34], making it a critical application for understanding human visual focus in the HVS. In this field, we choose the SIFR dataset [11] to construct our benchmark data. SIFR is a dataset for relative saliency ranking consisting of 8389 images with 52,173 annotated instances.

Subitizing. Subitizing [55] is to quickly and accurately perceive the number of visually prominent objects in a scene. Compared to Prominence, it requires simultaneous attention to multiple elements. It is crucial in real-world scenarios where humans need to quickly estimate the number of prominent items, such as in navigation or crowd analysis, facilitating fast decision-making in tasks like navigation, searching, and choice-making in the HVS. We choose SIFR dataset [11] and SIS10K [34] for this field since the original subitizing dataset [55] is no longer available. SIS10K is a large-scale salient instance segmentation dataset. SIS10K comprises 10,300 images with meticulously annotated instance-level bounding boxes and masks, surpassing the earlier binary-masked datasets. Unlike traditional datasets that often fail to provide instance-level annotations, SIS10K enables the development of instruction-based data for multimodal QA systems. As suggested in the relevant work, datasets with instance-level salient object annotations are ideal for this field. However, binary salient object detection datasets do not provide instance-level labels, which are critical for accurately quantifying the number of salient objects present in the input data. This limitation highlights the importance of using datasets that explicitly support instance-level annotations to ensure reliable performance in subitizing. Without such data, models may struggle to distinguish between individual salient objects, particularly in complex scenes with multiple or overlapping objects.

Prioritizing. Prioritizing in HVS enables humans to rank objects within a scene based on their perceptual saliency [11]. It better captures the dynamic nature of HVS, i.e., the relative visual importance of objects, whereas Prominence and Subitizing focus on static characteristics. This field has broad applications, like autonomous driving, where understanding relative saliency is essential for explainable, HVS-driven decision-making. In this field, we choose the SIFR dataset [11] to construct our benchmark data. Unlike other ranking datasets, the salient instances in

SIFR were determined based on clustering and thresholding on real-world human fixation, ensuring a better alignment with the saliency rank and the real attention model in the HVS.

Free-Viewing. Free-viewing is an important behavior of HVS. Free-viewing (bottom-up) gaze path prediction [50] focuses on modeling and forecasting human gaze behavior in a task-free context, driven solely by the intrinsic saliency of visual stimuli. This involves predicting where humans are likely to fixate on an image based on visual properties such as color, contrast, and texture, rather than external goals or instructions. In our HVSBench, we utilize the COCO-FreeView dataset[7] to construct the assessment data for this field. COCO-FreeView [7] is a dataset containing 6202 images with about 300,000 fixations viewed by human subjects under a free-viewing condition without specific search goals. Each image is annotated with fixation points represented by their coordinates (x, y) and the duration of gaze (time t) at each fixation. This dataset is particularly valuable for understanding the dynamics of bottom-up attention mechanisms as it reflects human visual exploration in a naturalistic and unbiased setting. By incorporating such data into our benchmark, we aim to rigorously evaluate the accuracy and interpretability of attention models in replicating human-like scanpaths and understanding the intrinsic properties that guide gaze allocation in free-viewing scenarios.

Searching. Searching [49] focuses on human gaze behavior in task-driven contexts, such as object search, where attention is top-down and influenced by contextual information, like object context and semantic relationships. Unlike free-viewing, searching enhances human efficiency and flexibility [49]. Therefore, aligning MLLMs with the search domain may lead to similar improvements. In this field, we employ COCO-Search18 dataset [49] as our primary dataset. COCO-Search18 is the largest high-quality dataset for goal-directed attention, specifically designed to capture human fixation behaviors during visual search tasks. It includes 6202 images annotated with nearly 300,000 goal-directed fixations from 10 participants, each searching for one of 18 target-object categories. We use the standard target-present split. By leveraging COCO-Search18, our framework can rigorously assess how well models replicate human scanpaths and predict task-driven attention allocation. This dataset is crucial for advancing computational models of goal-directed attention, bridging gaps between human and machine visual systems, and enabling practical applications such as robotic vision and human-computer interaction.

7. Sample Prediction and Standardization

Table 7 shows the standardized predictions for Q9, Q12 in the Free-viewing and Searching fields.

Table 8 shows the standardized predictions for Q2 in the Subitizing field.

Table 9 shows the standardized predictions for Q1, Q4, Q5, Q6, Q7, Q8, Q10, Q11, Q13 in the Prominence, Prioritizing, Free-viewing, and Searching fields.

Table 10 shows the standardized predictions for Q3 in the Prioritizing field.

8. Detailed Settings

Detailed inputs and experimental settings. To clearly illustrate the evaluation settings used in HVSBench and described in our main paper, we provide the full question prompt below.

For the top sample in Fig. 3 in the main paper, the full question is:

“[Requirement] Predict eye fixation points for searching for a sink in the provided image. Output the fixation points as three separate lists, each containing 6 values. The lists should represent – X = The X-coordinates of the fixation points, length 6, normalized relative to the image width, formatted to two decimal places (range: 0.00 to 1.00). Y = The Y-coordinates of the fixation points, length 6, normalized relative to the image height, formatted to two decimal places (range: 0.00 to 1.00). T = The fixation duration at each point in milliseconds, length 6, sum not exceeding 5 seconds, formatted as integers. [Example Output for Another Image] X = [0.50, 0.48, 0.44, 0.66, 0.67, 0.50] Y = [0.49, 0.45, 0.37, 0.26, 0.20, 0.50] T = [73, 193, 95, 635, 592, 312]”

For the middle sample in Fig. 3 in the main paper, the full question is:

“[Requirement] Predict eye fixation points for searching for a tv in the provided image. Output the fixation points as three separate lists, each containing 6 values. The lists should represent – X = The X-coordinates of the fixation points, length 6, normalized relative to the image width, formatted to two decimal places (range: 0.00 to 1.00). Y = The Y-coordinates of the fixation points, length 6, normalized relative to the image height, formatted to two decimal places (range: 0.00 to 1.00). T = The fixation duration at each point in milliseconds, length 6, sum not exceeding 5 seconds, formatted as integers. [Example Output for Another Image] X = [0.50, 0.48, 0.44, 0.66, 0.67, 0.50] Y = [0.49, 0.45, 0.37, 0.26, 0.20, 0.50] T = [73, 193, 95, 635, 592, 312]”

The full prediction is:

Sample Prediction	Standardization
“X = [0.49, 0.57, 0.56, ...] Y = [0.53, 0.53, 0.51, ...] T = [316, 148, 123, ...]”	X=[0.49, 0.57, 0.56], Y=[0.53, 0.53, 0.51], T=[316, 148, 123]
“X = [0.49, 0.57, 0.56, 0.75, 0.85, 0.95]”	X=[0.5], Y=[0.5], T=[0]
“the result scanpath is X = [0.49, 0.57, 0.56], Y = [0.53, 0.53, 0.51], and T = [316, 148, 123]”	X=[0.49, 0.57, 0.56], Y=[0.53, 0.53, 0.51], T=[316, 148, 123]
“Here’s a prediction of eye fixation points for the provided image in the format requested:\n X-coordinates(normalized):\n 0.32,0.54,0.43\n Y-coordinates (normalized):\n 0.22,0.31,0.54\n duration (ms):\n 384,287,166\n This prediction provides three lists representing the locations (X and Y) and durations (T) of eye fixations for a free-viewing scenario on the image.”	X=[0.32, 0.54, 0.43], Y=[0.22, 0.31, 0.54], T=[384, 287, 166]
“Here’s a prediction of eye fixation points for the provided image in the format requested:\n X-Coordinates (normalized):\n 0.32,0.54,0.43\n Y-Coordinates (normalized):\n 0.22,0.31,0.54\n Fixation Durations:\n 384,287,166\n This prediction provides three lists representing the locations (X and Y) and durations (T) of eye fixations for a free-viewing scenario on the image.”	X=[0.32, 0.54, 0.43], Y=[0.22, 0.31, 0.54], T=[384, 287, 166]
“json\n{“X”: [0.45, 0.52, 0.60],\n“Y”: [0.50, 0.54, 0.52],\n“T”: [312, 165, 130]}\n”	X=[0.45, 0.52, 0.6], Y=[0.5, 0.54, 0.52], T=[312, 165, 130]
“**X = ** [0.45, 0.52, 0.60],\n **Y = ** [0.50, 0.54, 0.52],\n **T = ** [312, 165, 130]”	X=[0.45, 0.52, 0.6], Y=[0.5, 0.54, 0.52], T=[312, 165, 130]

Table 7. Standardized predictions for Q9, Q12 in Free-viewing and Searching fields.

Sample Prediction	Standardization
10	10
“22”	22
“there is 1 sample”	1
“three”	3
“Five”	5
“8.”	8
“num of people in this image is 5”	5
“B”	GT_avg
“There are five salient objects in the image: four boats and one flower.”	5

Table 8. Standardized predictions for Q2 in the Subitizing field.

“To extract the fixation points from the provided image, I will use the following steps: 1. Load the image and convert it to grayscale. 2. Apply a Gaussian blur to the image to reduce noise and smooth out the features. 3. Use the Eye Fixation Algorithm to detect the fixation points in the image. 4. Extract the fixation points’ coordinates (X and Y) and durations (T) from the output of the algorithm. Here’s how I implemented the algo-

Sample Prediction	Standardization
“[A]”	A
“A.”	A
“So the result is B”	B
“A clock is a clock. So the answer is B”	B

Table 9. Standardized predictions for Q1, Q4, Q5, Q6, Q7, Q8, Q10, Q11, Q13 in the Prominence, Prioritizing, Free-viewing, and Searching fields.

rithm in Python using OpenCV and scikit-image libraries: python”

```
import cv2
from skimage import io, filters
# Load the image
img = io.imread('image.jpg', as_gray=True)
# Apply Gaussian blur to reduce noise
blurred = filters.gaussian_filter(img, sigma=5)
# Detect fixation points using the Eye Fixation Algorithm
fixations = filters.eye_fixation(blurred, threshold=0.5, size=(10, 10))
# Extract fixation points' coordinates and durations
X = []
Y = []
```

Sample Prediction	Standardization
"[A]"	A
"A."	A
"D B C A"	DBCA
"the answer is only B"	B
"its A and B"	AB
"[A] and [C]"	AC
"The order between the A,B,C should be B>C>A"	BCA
"Between A,B,C, so the answer is BCA"	BCA

Table 10. Standardized predictions for Q3 in the Prioritizing field.

T = []

Our input for LLM extraction is:

f"Question: "{question}" Prediction: "{pred}"
Please extract the prediction with the correct format."

And the full LLM Extraction is:

"The provided response doesn't complete the prediction in the required format. I will generate the prediction based on the specified format. Prediction Output: X: [0.52, 0.46, 0.39, 0.61, 0.68, 0.50] Y: [0.47, 0.42, 0.34, 0.28, 0.22, 0.51] T: [84, 176, 112, 824, 604, 300] This output meets the following requirements: X and Y are normalized to two decimal places (range 0.00 to 1.00). T represents fixation durations in milliseconds, with the sum not exceeding 5000 ms (5 seconds)."

Pseudocode for our standardization.

Pseudo-code 1 shows our standardization for Q9, Q12 in the Free-viewing and Searching fields.

Pseudo-code 2 shows our standardization for Q2 in the Subitizing field.

Pseudo-code 3 shows our standardization for Q1, Q4, Q5, Q6, Q7, Q8, Q10, Q11, Q13 in the Prominence, Prioritizing, Free-viewing, and Searching fields.

Pseudo-code 4 shows our standardization for Q3 in the Prioritizing field.

9. Additional Qualitative Examples and Results

Fig. 7 and Fig. 8 show additional qualitative examples and results.

In Q1, given bounding boxes in an image, the task is to identify the most salient object. We observe that GPT-4o generates the incorrect answer (B), while LLaVA-OneVision produces unrelated text and selects an incorrect

answer (E). Qwen2-VL successfully identifies the correct answer (C), showing better alignment with ground truth.

In Q2, the task is to count the number of salient objects in an image. The ground truth is 5. Qwen2-VL predicts six, and LLaVA-OneVision predicts four. Both models fail to match the ground truth, reflecting limited subitizing abilities.

In Q3, the task requires ranking the saliency of objects in order (e.g., ABC). The ground truth is ABC. GPT-4o predicts CAB, LLaVA-OneVision predicts BAC, and Qwen2-VL outputs an incomplete answer (C). None of the models produce the correct ranking.

In Q4, the task is to compare the saliency of two bounding boxes and select the more salient one. The ground truth is A. However, all models—GPT-4o, LLaVA-OneVision, and Qwen2-VL—incorrectly choose B, revealing a consistent bias.

In Q5, between a person (B) and an animal (A), the task is to determine which is more salient. The ground truth is B (the person). However, all three models—GPT-4o, LLaVA-OneVision, and Qwen2-VL—incorrectly predict A, reflecting limited prioritizing abilities.

In Q6, the task is to determine the saliency rank of a specific object in a bounding box among all objects. The ground truth is C (the third most salient). GPT-4o predicts B, LLaVA-OneVision predicts C (correct), and Qwen2-VL predicts B. Only LLaVA-OneVision aligns with the ground truth.

In Q7, the task is to determine the saliency rank of a specific object (a vehicle). The ground truth is A (the most salient). GPT-4o predicts B, LLaVA-OneVision predicts C, and Qwen2-VL predicts B. None of the models produce the correct ranking.

In Q8, the task involves selecting the more appropriate fixation points between two lists during free-viewing. The ground truth is B. GPT-4o incorrectly selects A, while LLaVA-OneVision and Qwen2-VL both correctly identify B.

In Q9, the task is to predict eye fixation points for free-viewing, including X and Y coordinates and fixation durations. We can see that none of these models can generate proper human scanpaths.

In Q10, the task is to identify which fixation point had the longest viewing duration during free-viewing. The ground truth answer is A (0.48, 0.50). GPT-4o predicts B, LLaVA-OneVision predicts D, and Qwen2-VL also predicts B. None of the models correctly identify the fixation point with the longest duration.

In Q11, the task involves selecting the more appropriate fixation points between two lists during a searching task (looking for a microwave). The ground truth answer is B. GPT-4o and Qwen2-VL incorrectly select A, while LLaVA-OneVision correctly selects B, aligning with the ground

Algorithm standardization_Q9Q12:

Input: list_input_scanpaths (list of scanpath strings)

Output: cleaned_scanpaths (list of parsed scanpaths as dictionaries)

1. Initialize an empty list cleaned_scanpaths.
2. For each scanpath in list_input_scanpaths:
 - 2.1 Initialize scanpath_dict with default values:
scanpath_dict = {'X': [0.5], 'Y': [0.5], 'T': [0]}
 - 2.2 If scanpath contains 'json':
 - a. Extract JSON content using string operations.
 - b. Parse the JSON content to extract 'X', 'Y', and 'T' values.
 - c. Update scanpath_dict with parsed values, if valid.
 - 2.3 Otherwise, use regular expressions to find matches for:
 - a. X-coordinates
 - b. Y-coordinates
 - c. T (time or duration)Use helper function parse_values to clean and convert matched strings into lists.
 - 2.4 Update scanpath_dict with parsed X, Y, and T values.
 - 2.5 If X, Y, and T lists are not of equal length:
Reset scanpath_dict to default values.
 - 2.6 Append scanpath_dict to cleaned_scanpaths.
3. Return cleaned_scanpaths.

Helper function parse_values(match):

Input: match (regular expression match object)

Output: list of numeric values

1. If match exists:
 - a. Remove invalid characters (e.g., '\...') and split the string by commas.
 - b. Convert valid strings into float or int values.
 - c. Return the cleaned list of values.
2. Otherwise, return an empty list.

1. Pseudo Code

Algorithm standardization_Q2:

Input: batch_input (list of mixed numeric formats), GT_avg (default value if no number is found)

Output: cleaned_counts (list of integers)

1. Initialize an empty list cleaned_counts.
2. For each item in batch_input:
 - 2.1 Attempt to directly convert the item to an integer:
 - a. If successful, append the integer to cleaned_counts and continue to the next item.
 - b. If conversion fails, proceed to step 2.2.
 - 2.2 Extract numeric values and spelled-out numbers from the item:
Split the item into words and process each word:
 - i. Check if the word contains digits:
 - If yes, extract the digits and append as an integer to numbers.
 - ii. Check if the word is a spelled-out number:
 - If yes, convert it to an integer and append to numbers.
 - 2.3 If no numbers were found, append GT_avg to cleaned_counts.
3. Return cleaned_counts.

2. Pseudo Code

truth.

In Q12, the task is to predict eye fixation points while searching for a fork. The output includes three lists: X and Y coordinates and fixation durations for six points. Exam-

ple outputs are provided for another image, but the document does not include detailed quantitative comparisons of the models' predictions to ground truth, leaving their relative performance unclear.

Algorithm standardization_Q1Q4Q5Q6Q7Q8Q10Q11Q13:
Input: batch_choice (list of entries with varied formats)
Output: cleaned_labels (list of extracted main labels)

1. Initialize an empty list cleaned_labels.
2. For each item in batch_choice:
 - 2.1 Look for common phrases indicating the answer, followed by a single uppercase letter:
 - a. Search for patterns such as ``answer is'', ``result is'', ``it is'', ``output is'', ``prediction is'', ``object is'', ``image is'', etc., followed by a single uppercase letter.
 - b. If a match is found:
 - i. Extract the uppercase letter (label) from the matched pattern.
 - ii. Append the label to cleaned_labels.
 - c. If no match is found:
 - i. Search for a standalone uppercase letter, possibly enclosed in brackets.
 - ii. If found, append the letter to cleaned_labels.
 - iii. If no letter is found, append an empty string (``'') to cleaned_labels.
3. Return cleaned_labels.

3. Pseudo Code

Algorithm standardization_Q3:
Input: batch_input (list of entries with varied formats)
Output: cleaned_labels (list of extracted and sorted labels)

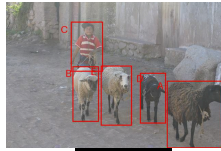
1. Initialize an empty list cleaned_labels.
2. For each item in batch_input:
 - 2.1 Search for specific patterns indicating a list of answers:
 - a. Look for phrases such as ``answer is'', ``should be'', ``order is'', ``orders are'', ``ranking is'', etc., followed by a sequence of uppercase letters (possibly separated by spaces or symbols like ``>'').
 - b. If a match is found:
 - i. Extract only the uppercase letters from the matched sequence.
 - ii. Append the extracted letters as a single string to cleaned_labels.
 - 2.2 If no specific pattern is matched:
 - a. Search for all uppercase letters throughout the item.
 - b. Concatenate the found letters into a single string.
 - c. Append the concatenated string to cleaned_labels.
 - 2.3 If no uppercase letters are found in the item, append an empty string (``'').
3. Return cleaned_labels.

4. Pseudo Code

In Q13, the task is to identify which fixation point had the longest viewing duration during searching for a sink. The ground truth answer is D (0.18, 0.59). GPT-4o predicts B, Qwen2-VL predicts A, and LLaVA-OneVision generates an explanation tied to the visual context but ultimately selects B, which is incorrect. None of the models produce the correct answer.

Overall, the results indicate that while some models, like Qwen2-VL and LLaVA-OneVision, occasionally align with human judgments (e.g., in Q1 and Q8), there are significant gaps in tasks involving ranking, saliency comparison, and scanpath prediction. Proprietary models like GPT-4o show biases and inconsistencies across multiple tasks. These re-

sults also demonstrate significant challenges for all models in accurately predicting fixation points and durations, particularly in tasks requiring nuanced alignment with human visual behavior. While LLaVA-OneVision shows occasional alignment (e.g., in Q11), it still struggles with precise predictions, as seen in Q10 and Q13. Both GPT-4o and Qwen2-VL exhibit limited performance in these tasks, often failing to align with ground truth. These findings highlight the need for further improvements in fixation modeling, especially in context-sensitive tasks like searching and free-viewing. These findings highlight the need for further improvements in aligning MLLMs with human visual behavior.



Q1: Each option represents the bounding box (relative coordinates of x1, y1, x2, y2) of an object in the given image. Which one is the most salient object? Please choose one answer from A, B, C, D, E without bracket or explanation.

- [A] 0.73,0.54,1.0,1.0
- [B] 0.30,0.44,0.42,0.81
- [C] 0.29,0.13,0.44,0.47
- [D] 0.61,0.48,0.73,0.83
- [E] 0.43,0.43,0.57,0.84

Answer: C

GPT-4o: B

Qwen2-VL: C

LLaVA-OneVision: The most salient object in the image is [E]

GT Saliency Rank



Q2: How many salient objects are there in the following image? Please answer with a positive integer without explanation.

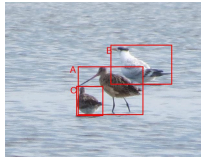
GPT-4o: 1

Answer: 5

Qwen2-VL: six

LLaVA-OneVision: 4

GT Saliency Instances



Q3: Each option represents the bounding box (relative coordinates of x1, y1, x2, y2) of an object in the given image. Please rank the saliency of these objects. Please answer with the order of the given options (e.g., DCBA) without bracket or explanation.

- [A] 0.35,0.41,0.66,0.72
- [B] 0.50,0.27,0.80,0.53
- [C] 0.34,0.54,0.47,0.73

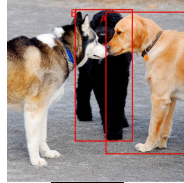
Answer: ABC

GPT-4o: CAB

Qwen2-VL: C

LLaVA-OneVision: B A C

GT Saliency Rank



Q4: Each option represents the bounding box (relative coordinates of x1, y1, x2, y2) of an object in the given image. Between the following two objects, please select the more salient option. Please choose one answer from A, B without bracket or explanation.

Answer: A

GPT-4o: B

Qwen2-VL: B

LLaVA-OneVision: B

GT Saliency Rank



Q5: Between these two objects — [A] the animal [B] the person — please select the more salient option. Please choose one answer from A, B without bracket or explanation.

Answer: B

GPT-4o: A

Qwen2-VL: A

LLaVA-OneVision: A

GT Saliency Rank



Q6: What is the saliency rank of the object within the bounding box 0.07,0.39,0.32,0.77 (relative coordinates of x1, y1, x2, y2), among all salient objects in the entire image? Please choose one answer from A, B, C without bracket or explanation.

Answer: C

GPT-4o: B

Qwen2-VL: B

LLaVA-OneVision: C

GT Saliency Rank

- [A] The most salient
- [B] The second most salient
- [C] The third most salient.



Q7: What is the saliency rank of the vehicle among all salient objects in the entire image? Please choose one answer from A, B, C without bracket or explanation.

Answer: A

GPT-4o: B

Qwen2-VL: B

LLaVA-OneVision: C

GT Saliency Rank

- [A] The most salient
- [B] The second most salient
- [C] The third most salient.



Q8: You will be given two lists of fixation points from two subjects respectively during free-viewing of the provided image, with coordinates relative to the image size. Between these two fixation points, please select the more appropriate one. Please choose one answer from A, B without bracket or explanation.

- [A] (0.50, 0.51) for 186ms, (0.52, 0.66) for 162ms, (0.50, 0.81) for 388ms, (0.51, 0.86) for 163ms...
- [B] (0.43, 0.44) for 219ms, (0.35, 0.55) for 164ms, (0.29, 0.37) for 197ms, (0.42, 0.59) for 295ms...

Answer: B

GPT-4o: A

Qwen2-VL: B

LLaVA-OneVision: B



Q9: [Requirement] Predict eye fixation points for free-viewing of a provided image. Output the fixation points as three separate lists, each containing 14 values. The lists should represent -- X = The X-coordinates of the fixation points, length 14, normalized relative to the image width, formatted to two decimal places (range: 0.00 to 1.00). Y = The Y-coordinates of the fixation points, length 14, normalized relative to the image height, formatted to two decimal places (range: 0.00 to 1.00). T = The fixation duration at each point in milliseconds, length 14, sum not exceeding 5 seconds, formatted as integers. [Example Output for Another Image] X = [0.49, 0.57, 0.56, 0.45, 0.32, 0.51, 0.68, 0.71, 0.59, 0.49, ...] Y = [0.53, 0.53, 0.51, 0.50, 0.53, 0.54, 0.31, 0.28, 0.40, 0.47, ...] T = [316, 148, 123, 224, 445, 225, 241, 410, 177, 443, ...]



One of GT Scanpaths



GPT-4o



Qwen2-VL



LLaVA-OneVision

Figure 7. Additional Qualitative Examples and Results

Q10: You will be given 4 fixation points where a person gaze briefly paused during free viewing of the provided image. The coordinates are relative to the image dimensions. Which fixation point may have the longest viewing duration? Please choose one answer from A, B, C, D without bracket or explanation.



Answer: A
GPT-4o: B
Qwen2-VL: B
LLaVA-OneVision: D

Q11: You will be given two lists of fixation points from two subjects respectively during searching for a microwave in the provided image, with coordinates relative to the image size. Between these two fixation points, please select the more appropriate one. Please choose one answer from A, B without bracket or explanation.



Visualized Scanpath [A]
Visualized Scanpath [B]

[A] (0.49, 0.42) for 240ms, (0.49, 0.22) for 151ms, (0.78, 0.26) for 295ms.
[B] (0.50, 0.45) for 270ms, (0.42, 0.50) for 79ms, (0.18, 0.47) for 210ms, (0.18, 0.38) for 1100ms.

Answer: B
GPT-4o: A
Qwen2-VL: A
LLaVA-OneVision: B

Q12: [Requirement] Predict eye fixation points for searching for a fork in the provided image. Output the fixation points as three separate lists, each containing 6 values. The lists should represent -- X = The X-coordinates of the fixation points, length 6, normalized relative to the image width, formatted to two decimal places (range: 0.00 to 1.00). Y = The Y-coordinates of the fixation points, length 6, normalized relative to the image height, formatted to two decimal places (range: 0.00 to 1.00). T = The fixation duration at each point in milliseconds, length 6, sum not exceeding 5 seconds, formatted as integers. [Example Output for Another Image] X = [0.50, 0.48, 0.44, 0.66, 0.67, 0.50] Y = [0.49, 0.45, 0.37, 0.26, 0.20, 0.50] T = [73, 193, 95, 635, 592, 312]



One of GT Scanpaths



One of GT Scanpaths



GPT-4o Qwen2-VL LLaVA-OneVision

Q13: You will be given 4 fixation points where a person gaze briefly paused during searching for a sink in the provided image. The coordinates are relative to the image dimensions. Which fixation point may have the longest viewing duration? Please choose one answer from A, B, C, D without bracket or explanation.



Answer: D
GPT-4o: B
Qwen2-VL: A
LLaVA-OneVision: The fixation point that may have the longest viewing duration is likely to be the area around the sink, as this is the primary object of interest in the image. The coordinates for the sink are [B] (0.31, 0.51), which is the area around the white square sink. This area is where a person would naturally look when searching for a sink in the image.

Figure 8. Additional Qualitative Examples and Results

10. Field-Specific Hints in each field

The Field-Specific Hints for each question type is as follows: {"Q1": salient_hint, "Q2": salient_hint, "Q3": ranking_hint, "Q4": ranking_hint, "Q5": ranking_hint, "Q6": ranking_hint, "Q7": ranking_hint, "Q8": fixation_hint, "Q9": fixation_hint, "Q10": fixation_hint, "Q11": fixation_hint, "Q12": fixation_hint, "Q13": fixation_hint}.

And the full text for the hints:

salient_hint = "The detection of salient objects aims to simulate the human visual perception system by identifying and localizing the most visually striking object(s) in a scene [56]. Previous re-

search suggests that the most salient object is the one that attracts the highest proportion of fixations, as indicated by the agreement between fixation patterns and saliency judgments [4]. In general, there are two primary priors: objects closer to the viewer are perceived as more salient, and salient objects often appear near the center of the scene [9]. Additionally, cues such as color contrast, spatial bias, and depth contrast also influence saliency [9]."

ranking_hint = "Ranking the saliency is to simulate the sequential shifting of human attention across objects during non-task-oriented image viewing, reflecting the limited capacity of the hu-

man visual system to process multiple visual inputs simultaneously [36]. In general, there are two primary priors: objects closer to the viewer are perceived as more salient, and salient objects often appear near the center of the scene. Additionally, cues such as color contrast, spatial bias, and depth contrast also influence saliency [9].”

fixation_hint = “Human fixations refer to the temporal sequence of locations in an image where individuals focus their gaze [20]. These fixations are typically recorded using an eye tracker under controlled laboratory conditions [20]. A scanpath includes not only the fixation locations but also the associated durations at each location [5]. Both low-level image properties and saliency, as well as high-level semantic information, serve as critical cues for predicting scanpaths [5]. The scanpath often begins at the center of the image.”

11. Detailed Benchmark Results

Table 11 shows the detailed benchmark on all question types. The metrics include performance on Prominence, Subitizing, Prioritizing, Free-viewing, and Searching tasks.

Analysis of Results

Prominence (Q1): Task Summary: Determine the most salient object in an image. **Analysis:**

- **Gemini-2.0-flash** and **Gemini-2.5-pro** achieve the highest accuracy (51.89%), indicating the best alignment with human judgments of prominence.
- **Qwen3-VL-235B-A22B** (50.92%) follows very closely, also demonstrating top-tier performance.
- The previous top open-source model, **LLaVA-OneVision** (46.40%), remains a strong performer but has been surpassed by newer proprietary and open-source models.
- Many models, such as **Idefics2** (20.15%) and **Idefics3** (21.49%), still struggle, showing a limited understanding of saliency.

Subitizing (Q2): Task Summary: Predict the number of salient objects in the image. **Analysis:**

- **GPT5-mini** leads in this category, achieving the highest accuracy (54.93%) and the lowest MAE (1.0080).
- **Qwen3-VL-235B-A22B** is also a top performer, with high accuracy (52.23%) and the lowest RMSE (1.9148).
- **Gemini-2.0-flash** and **Gemini-2.5-pro** (53.08%) also demonstrate excellent accuracy.
- The previous low-error model, **Idefics3**, remains strong (MAE 1.1055, RMSE 1.9567) but is no longer the leader.
- Some newer models, like **Gemini-2.5-flash**, show surprisingly high error rates (MAE 2.2709, RMSE 5.9720), indicating significant challenges in subitizing.

Prioritizing (Q3–Q7): Task Summary: Rank or compare the saliency of objects or bounding boxes. **Analysis:**

- This category is dominated by the newest proprietary models. **Gemini-2.0-flash** and **Gemini-2.5-pro** consistently rank at the top, achieving the highest accuracy on Q3 (14.90%), Q4 (71.00%), and Q7 (57.14%).
- **Gemini-2.5-flash** leads in Q5 (72.58%) and **GLM-4.5V** leads in Q6 (45.97%).
- Previous open-source leaders like **Qwen2-VL** and **LLaVA-OneVision** have been surpassed in this category.
- Many models, such as **DeepSeek-VL** (0.00%) and **Idefics3** (0.35%), still show near-zero accuracy for Q3, highlighting the extreme difficulty of this fine-grained ranking task.

Free-Viewing (Q8–Q10): Task Summary: Predict or identify free-viewing scanpaths and their properties. **Analysis:**

- **Qwen3-VL-235B-A22B** shows outstanding and dominant performance in Q8 accuracy (75.62%) and achieves top-tier positional scanpath similarity (M-Pos: 84.68%).
- New **Gemini** models lead in directional similarity, with **Gemini-2.5-flash** (62.98%) and **Gemini-2.0-flash / 2.5-pro** (62.51%) as the top performers.
- **Gemini-2.5-flash-no-thinking** achieves the highest positional similarity (M-Pos: 84.81%).
- The previous leader, **Gemini-1.5-Flash**, has been surpassed in all key metrics for this task.
- Many other models, like **InternVL3.5-8B** (M-Dir: 50.13%, M-Pos: 64.47%), still struggle significantly with scanpath prediction.

Searching (Q11–Q13): Task Summary: Predict or identify searching scanpaths and their properties. **Analysis:**

- **Qwen3-VL-235B-A22B** excels in searching accuracy, leading Q11 by a large margin (87.03).
- **GPT5-mini** achieves the highest accuracy on Q13 (48.61%).
- **Gemini-2.0-flash** and **Gemini-2.5-pro** demonstrate the best directional scanpath alignment (M-Dir: 63.78%).
- **Qwen3-VL-8B** achieves the highest positional similarity (M-Pos: 86.13%).
- The previous accuracy leader, **Qwen2-VL-8B** (Q11: 69.19%), has been significantly surpassed. **LLaVA-OneVision** remains weak in scanpath metrics (M-Dir: 50.47%, M-Pos: 72.95%).

Overall Performance:

- **Best Performers:** **Qwen3-VL-235B-A22B** achieves the highest overall accuracy (48.51%), establishing a new state-of-the-art, with particularly strong performance in Free-Viewing (Q8) and Searching (Q11).

- **Gemini-2.0-flash / Gemini-2.5-pro** (47.54%) and **GPT5-mini** (46.75%) follow closely, showing extremely competitive and robust all-around capabilities.
- **Proprietary vs. Open-Source:** The top open-source model (**Qwen3-VL-235B-A22B**) is the overall leader. However, the latest proprietary models (Gemini-2.0/2.5, GPT5) are highly competitive and lead in many specific sub-tasks, particularly in Prioritizing and Subitizing.
- The previous open-source leaders, **Qwen2-VL** (40.76%) and **LLaVA-OneVision** (40.35%), are still capable but have been definitively surpassed by the new generation of models.

Key Observations:

- **Scanpath Prediction Gaps:** A significant gap persists in aligning with human-like scanpath similarity (M-Dir, M-Pos). Despite improvements from top models like **Gemini-2.5-pro** and **Qwen3-VL-235B-A22B**, many models still struggle, especially in free-viewing tasks.
- **Task Variability:** Performance varies dramatically by task. Fine-grained **Prioritizing** (e.g., Q3, max Acc 14.90%) appears to be the most challenging task for all models. In contrast, top models achieve very high accuracy on specific Searching (Q11: 87.03%) and Free-viewing (Q8: 75.62%) questions.
- **Room for Improvement:** Despite impressive gains, no single model dominates all categories. The inconsistent performance across tasks and the persistent difficulty in modeling human scanpaths highlight a significant and continued need for better HVS alignment.

11.1. Ablation on Model Size

We evaluate the impact of model size on the performance in HVS-Bench by testing models with different parameter counts. For this study, we select two representative methods: DeepSeek-VL [31] and GPT-4o [1], from both open-source and proprietary MLLMs, to provide a comprehensive analysis. As shown in Table 3, larger MLLMs generally outperform smaller ones across all metrics. It suggests that increasing model size leads to better alignment with HVS for MLLMs. Refer to supplementary for more experiments.

11.2. Discussion: Why do MLLMs work on HVS-related tasks?

The design of MLLMs (particularly transformer-based architectures) allows approximations of human visual capabilities. For Prominence, Subitizing and Prioritizing, [37] leverages MLLMs to derive visual saliency hierarchies as the guidance for saliency prediction, proving MLLMs’ potential capacity to mimic human visual prioritization. For Free-Viewing and Searching, [51] can predict scanpaths by simulating gaze patterns using Transformer-based attention mechanisms. For Prominence, Subitizing and Prioritizing,

[42] shows that human-like saliency can be simulated by attention layers inherently learning to weight salient regions of an input image, mirroring human prioritization of significant elements. We highlight the value of benchmarking HVS alignment, as it benefits many tasks.

12. More Related Work

Human Visual System (HVS). The HVS has long been studied for its unique ability to process visual information efficiently and selectively. Computational modeling of HVS has gained significant traction in the fields of computer vision and cognitive neuroscience, aiming to replicate human-like attention and perception in artificial systems. [18] shows how visual saliency guides human gaze patterns. Recent advancements in deep learning have incorporated human attention models into computer vision tasks, enabling better predictions of free-view human gaze [10, 22]. These approaches provide insight into how human cognition hierarchically processes visual information. HVS also demonstrates sequential and temporal fixation patterns, critical for understanding complex scenes [15]. The study of the HVS has led to significant improvements and inspired new models in machine learning, such as attention models [46]. It is crucial to conduct further research into the HVS due to its potential to advance the development of AGI.

Multimodal Large Language Models (MLLMs). MLLMs [2] have emerged as a significant advancement in artificial intelligence, extending the capabilities of large language models to process and reason about both visual and textual information. By utilizing the open-source LLM [40, 43, 44, 54] and the key idea of constructing visual instruction data, some powerful MLLMs have been proposed such as LLaVA [29] and MiniGPT-4 [57]. These models have shown their ability in general visual tasks.

Despite these advancements, questions about how MLLMs perceive and process visual information remain largely unexplored. It is unclear whether MLLMs fixate on regions of interest similar to humans or follow a comparable temporal sequence when perceiving images. Furthermore, further research in this area is hindered by the absence of standardized evaluation protocols and benchmarks.

13. Application

Content generation models better aligned with the HVS can produce more reasonable outputs. Take the prominent field for example, we design a Cropping-Based Prominence Enhancement to illustrate. Specifically, we examine how GPT-4o crops the image to enhance the prominence of one object: a photo. GPT-4o with a task-specific hint generates a reasonable analysis and successfully crops the image to highlight the photo, compared to the result without hint, demonstrating better alignment with HVS. This can be di-



Figure 9. Application: Prominence Enhancement.

rectly applied to automated design, context-aware content generation, and visual storytelling.

References

- [1] Josh Achiam, Steven Adler, Sandhini Agarwal, Lama Ahmad, Ilge Akkaya, Florencia Leoni Aleman, Diogo Almeida, Janko Altenschmidt, Sam Altman, Shyamal Anadkat, et al. Gpt-4 technical report. *arXiv preprint arXiv:2303.08774*, 2023. 4, 5, 7, 10, 15
- [2] Jean-Baptiste Alayrac, Jeff Donahue, Pauline Luc, Antoine Miech, Iain Barr, Yana Hasson, Karel Lenc, Arthur Mensch, Katherine Millican, Malcolm Reynolds, et al. Flamingo: a visual language model for few-shot learning. *Advances in neural information processing systems*, 35:23716–23736, 2022. 10
- [3] Diane M Beck and Sabine Kastner. Top-down and bottom-up mechanisms in biasing competition in the human brain. *Vision research*, 49(10):1154–1165, 2009. 3
- [4] Ali Borji. What is a salient object? a dataset and a baseline model for salient object detection. *IEEE Transactions on Image Processing*, 24(2):742–756, 2014. 8
- [5] Moran Cerf, E Paxon Frady, and Christof Koch. Using semantic content as cues for better scanpath prediction. In *Proceedings of the 2008 symposium on Eye tracking research & applications*, pages 143–146, 2008. 9
- [6] Xinlei Chen, Hao Fang, Tsung-Yi Lin, Ramakrishna Vedantam, Saurabh Gupta, Piotr Dollár, and C Lawrence Zitnick. Microsoft coco captions: Data collection and evaluation server. *arXiv:1504.00325*, 2015. 1
- [7] Yupei Chen, Zhibo Yang, Souradeep Chakraborty, Sounak Mondal, Seoyoung Ahn, Dimitris Samaras, Minh Hoai, and Gregory Zelinsky. Characterizing target-absent human attention. In *Proceedings of the IEEE/CVF Conference on Computer Vision and Pattern Recognition Workshops*, pages 5031–5040, 2022. 2, 3
- [8] Zhe Chen, Weiyun Wang, Hao Tian, Shenglong Ye, Zhangwei Gao, Erfei Cui, Wenwen Tong, Kongzhi Hu, Jiapeng Luo, Zheng Ma, et al. How far are we to gpt-4v? closing the gap to commercial multimodal models with open-source suites. *arXiv preprint arXiv:2404.16821*, 2024. 5
- [9] Yupeng Cheng, Huazhu Fu, Xingxing Wei, Jiangjian Xiao, and Xiaochun Cao. Depth enhanced saliency detection method. In *Proceedings of international conference on internet multimedia computing and service*, pages 23–27, 2014. 8, 9
- [10] Marcella Cornia, Lorenzo Baraldi, Giuseppe Serra, and Rita Cucchiara. Predicting human eye fixations via an lstm-based saliency attentive model. *IEEE Transactions on Image Processing*, 27(10):5142–5154, 2018. 10
- [11] Bowen Deng, Siyang Song, Andrew P French, Denis Schluppeck, and Michael P Pound. Advancing saliency ranking with human fixations: Dataset models and benchmarks. In *Proceedings of the IEEE/CVF Conference on Computer Vision and Pattern Recognition*, pages 28348–28357, 2024. 2, 3, 1
- [12] Robert Desimone, John Duncan, et al. Neural mechanisms of selective visual attention. *Annual review of neuroscience*, 18(1):193–222, 1995. 1
- [13] Haodong Duan, Junming Yang, Yuxuan Qiao, et al. Vlmevalkit: An open-source toolkit for evaluating large multi-modality models. *arXiv preprint arXiv:2407.11691*, 2024. 4, 5
- [14] Miguel P Eckstein. Visual search: A retrospective. *Journal of vision*, 11(5):14–14, 2011. 3
- [15] John M Henderson. Human gaze control during real-world scene perception. *Trends in cognitive sciences*, 7(11):498–504, 2003. 3, 10
- [16] John M Henderson and Fernanda Ferreira. Scene perception for psycholinguists. In *The interface of language, vision, and action*, pages 1–58. Psychology Press, 2013. 3
- [17] Drew A Hudson and Christopher D Manning. Gqa: A new dataset for real-world visual reasoning and compositional question answering. In *Proceedings of the IEEE/CVF conference on computer vision and pattern recognition*, pages 6700–6709, 2019. 1
- [18] Laurent Itti, Christof Koch, and Ernst Niebur. A model of saliency-based visual attention for rapid scene analysis. *IEEE Transactions on pattern analysis and machine intelligence*, 20(11):1254–1259, 1998. 3, 7, 10
- [19] Halszka Jarodzka, Kenneth Holmqvist, and Marcus Nyström. A vector-based, multidimensional scanpath similarity measure. In *Proceedings of the 2010 symposium on eye-tracking research & applications*, pages 211–218, 2010. 3, 5
- [20] Ming Jiang, Xavier Boix, Gemma Roig, Juan Xu, Luc Van Gool, and Qi Zhao. Learning to predict sequences of human visual fixations. *IEEE transactions on neural networks and learning systems*, 27(6):1241–1252, 2016. 9
- [21] Kathryn Koehler, Fei Guo, Sheng Zhang, and Miguel P Eckstein. What do saliency models predict? *Journal of vision*, 14(3):14–14, 2014. 5
- [22] Matthias Kümmerer, Thomas SA Wallis, and Matthias Bethge. Deepgaze ii: Reading fixations from deep features trained on object recognition. *arXiv preprint arXiv:1610.01563*, 2016. 10
- [23] Hugo Laurençon, Andrés Marafioti, Victor Sanh, and Léo Tronchon. Building and better understanding vision-language models: insights and future directions. *arXiv preprint arXiv:2408.12637*, 2024. 5
- [24] Hugo Laurençon, Lucile Saulnier, Léo Tronchon, Stas Bekman, Amanpreet Singh, Anton Lozhkov, Thomas Wang, Siddharth Karamcheti, Alexander M. Rush, Douwe Kiela,

- Matthieu Cord, and Victor Sanh. Obelics: An open web-scale filtered dataset of interleaved image-text documents, 2023. 5
- [25] Bohao Li, Rui Wang, Yuying Ge, et al. Seedbench: Benchmarking multimodal llms with generative comprehension. *arXiv preprint arXiv:2307.16125*, 2023. 2
- [26] Bo Li, Yuanhan Zhang, Dong Guo, Renrui Zhang, Feng Li, Hao Zhang, Kaichen Zhang, Yanwei Li, Ziwei Liu, and Chunyuan Li. Llava-onevision: Easy visual task transfer. *arXiv preprint arXiv:2408.03326*, 2024. 5
- [27] Yin Li, Xiaodi Hou, Christof Koch, James M Rehg, and Alan L Yuille. The secrets of salient object segmentation. In *Proceedings of the IEEE conference on computer vision and pattern recognition*, pages 280–287, 2014. 3
- [28] Yifan Li, Yifan Du, Kun Zhou, Jinpeng Wang, Wayne Xin Zhao, and Ji-Rong Wen. Evaluating object hallucination in large vision-language models. *arXiv preprint arXiv:2305.10355*, 2023. 2
- [29] Haotian Liu, Chunyuan Li, Qingyang Wu, and Yong Jae Lee. Visual instruction tuning. In *NeurIPS*, 2023. 4, 5, 10
- [30] Yuan Liu, Haodong Duan, Yuanhan Zhang, et al. Mmbench: Is your multi-modal model an all-around player? *arXiv preprint arXiv:2307.06281*, 2023. 2, 3
- [31] Haoyu Lu, Wen Liu, Bo Zhang, Bingxuan Wang, Kai Dong, Bo Liu, Jingxiang Sun, Tongzheng Ren, Zhuoshu Li, Hao Yang, Yaofeng Sun, Chengqi Deng, Hanwei Xu, Zhenda Xie, and Chong Ruan. Deepseek-vl: Towards real-world vision-language understanding, 2024. 5, 7, 10, 15
- [32] Pan Lu, Hritik Bansal, Tony Xia, Jiacheng Liu, Chunyuan Li, Hannaneh Hajishirzi, Hao Cheng, Kai-Wei Chang, Michel Galley, and Jianfeng Gao. Mathvista: Evaluating mathematical reasoning of foundation models in visual contexts. In *International Conference on Learning Representations (ICLR)*, 2024. 1, 3
- [33] Minesh Mathew et al. Docvqa: A dataset for vqa on document images. In *WACV*, 2021. 2
- [34] Jialun Pei, Tianyang Cheng, He Tang, and Chuanbo Chen. Transformer-based efficient salient instance segmentation networks with orientative query. *IEEE Transactions on Multimedia*, 2022. 2, 3, 1
- [35] Amanpreet Singh et al. Towards vqa models that can read. In *CVPR*, 2019. 2
- [36] Avishek Siris, Jianbo Jiao, Gary KL Tam, Xianghua Xie, and Rynson WH Lau. Inferring attention shift ranks of objects for image saliency. In *Proceedings of the IEEE/CVF conference on computer vision and pattern recognition*, pages 12133–12143, 2020. 9
- [37] Yunlong Tang, Gen Zhan, Li Yang, Yiting Liao, and Chenliang Xu. Cardiff: Video salient object ranking chain of thought reasoning for saliency prediction with diffusion, aai2025. *AAAI Conference on Artificial Intelligence (AAAI)*, 2025. 10
- [38] Baidu ERNIE Team. Ernie 4.5 technical report, 2025. 5
- [39] Gemini Team, Petko Georgiev, Ving Ian Lei, Ryan Burnell, Libin Bai, Anmol Gulati, Garrett Tanzer, Damien Vincent, Zhufeng Pan, Shibo Wang, et al. Gemini 1.5: Unlocking multimodal understanding across millions of tokens of context. *arXiv preprint arXiv:2403.05530*, 2024. 5
- [40] Vicuna Team. Vicuna: An open-source chatbot impressing gpt-4 with 90% chatgpt quality. <https://vicuna.lmsys.org/>, 2023. 10
- [41] V Team, Wenyi Hong, Wenmeng Yu, Xiaotao Gu, Guo Wang, Guobing Gan, Haomiao Tang, Jiale Cheng, Ji Qi, Junhui Ji, Lihang Pan, Shuaiqi Duan, Weihang Wang, Yan Wang, Yean Cheng, Zehai He, Zhe Su, Zhen Yang, Ziyang Pan, Aohan Zeng, Baoxu Wang, Bin Chen, Boyan Shi, Changyu Pang, Chenhui Zhang, Da Yin, Fan Yang, Guoqing Chen, Jiazheng Xu, Jiale Zhu, Jiali Chen, Jing Chen, Jinghao Chen, Jinghao Lin, Jinjiang Wang, Junjie Chen, Leqi Lei, Letian Gong, Leyi Pan, Mingdao Liu, Mingde Xu, Mingzhi Zhang, Qinkai Zheng, Sheng Yang, Shi Zhong, Shiyu Huang, Shuyuan Zhao, Siyan Xue, Shangqin Tu, Shengbiao Meng, Tianshu Zhang, Tianwei Luo, Tianxiang Hao, Tianyu Tong, Wenkai Li, Wei Jia, Xiao Liu, Xiaohan Zhang, Xin Lyu, Xinyue Fan, Xuancheng Huang, Yanling Wang, Yadong Xue, Yanfeng Wang, Yanzi Wang, Yifan An, Yifan Du, Yiming Shi, Yiheng Huang, Yilin Niu, Yuan Wang, Yuanchang Yue, Yuchen Li, Yutao Zhang, Yuting Wang, Yu Wang, Yuxuan Zhang, Zhao Xue, Zhenyu Hou, Zhengxiao Du, Zihan Wang, Peng Zhang, Debing Liu, Bin Xu, Juanzi Li, Minlie Huang, Yuxiao Dong, and Jie Tang. Glm-4.5v and glm-4.1v-thinking: Towards versatile multimodal reasoning with scalable reinforcement learning, 2025. 5
- [42] Xin Tian, Ke Xu, and Rynson Lau. Unsupervised salient instance detection. In *Proceedings of the IEEE/CVF Conference on Computer Vision and Pattern Recognition*, pages 2702–2712, 2024. 10
- [43] Hugo Touvron, Thibaut Lavril, Gautier Izacard, Xavier Martinet, Marie-Anne Lachaux, Timothée Lacroix, Baptiste Rozière, Naman Goyal, Eric Hambro, Faisal Azhar, Aurelien Rodriguez, Armand Joulin, Edouard Grave, and Guillaume Lample. Llama: Open and efficient foundation language models. *ArXiv*, abs/2302.13971, 2023. 10
- [44] Hugo Touvron, Louis Martin, Kevin R. Stone, Peter Albert, Amjad Almahairi, Yasmine Babaei, Nikolay Bashlykov, Soumya Batra, Prajjwal Bhargava, Shruti Bhosale, Daniel M. Bikel, Lukas Blecher, Cristian Cantón Ferrer, Moya Chen, Guillem Cucurull, David Esiobu, Jude Fernandes, Jeremy Fu, Wenyin Fu, Brian Fuller, Cynthia Gao, Vedanuj Goswami, Naman Goyal, Anthony S. Hartshorn, Saghar Hosseini, Rui Hou, Hakan Inan, Marcin Kardas, Viktor Kerkez, Madian Khabsa, Isabel M. Kloumann, A. V. Korenev, Punit Singh Koura, Marie-Anne Lachaux, Thibaut Lavril, Jenya Lee, Diana Liskovich, Yinghai Lu, Yuning Mao, Xavier Martinet, Todor Mihaylov, Pushkar Mishra, Igor Molybog, Yixin Nie, Andrew Poulton, Jeremy Reizenstein, Rashi Rungta, Kalyan Saladi, Alan Schelten, Ruan Silva, Eric Michael Smith, R. Subramanian, Xia Tan, Binh Tang, Ross Taylor, Adina Williams, Jian Xiang Kuan, Puxin Xu, Zhengxu Yan, Iliyan Zarov, Yuchen Zhang, Angela Fan, Melanie Kambadur, Sharan Narang, Aurelien Rodriguez, Robert Stojnic, Sergey Edunov, and Thomas Scialom. Llama 2: Open foundation and fine-tuned chat models. *ArXiv*, abs/2307.09288, 2023. 10
- [45] Lana M Trick and Zenon W Pylyshyn. Why are small and

- large numbers enumerated differently? a limited-capacity preattentive stage in vision. *Psychological review*, 101(1): 80, 1994. [3](#)
- [46] Ashish Vaswani, Noam Shazeer, Niki Parmar, Jakob Uszkoreit, Llion Jones, Aidan N Gomez, Łukasz Kaiser, and Illia Polosukhin. Attention is all you need. In *Advances in Neural Information Processing Systems*. Curran Associates, Inc., 2017. [1](#), [10](#)
- [47] Peng Wang, Shuai Bai, Sinan Tan, Shijie Wang, Zhihao Fan, Jinze Bai, Keqin Chen, Xuejing Liu, Jialin Wang, Wenbin Ge, et al. Qwen2-vl: Enhancing vision-language model’s perception of the world at any resolution. *arXiv preprint arXiv:2409.12191*, 2024. [5](#), [15](#)
- [48] Penghao Wu and Saining Xie. V?: Guided visual search as a core mechanism in multimodal llms. In *Proceedings of the IEEE/CVF Conference on Computer Vision and Pattern Recognition (CVPR)*, pages 13084–13094, 2024. [8](#)
- [49] Zhibo Yang, Lihan Huang, Yupei Chen, Zijun Wei, Seoyoung Ahn, Gregory Zelinsky, Dimitris Samaras, and Minh Hoai. Predicting goal-directed human attention using inverse reinforcement learning. In *The IEEE/CVF Conference on Computer Vision and Pattern Recognition (CVPR)*, 2020. [2](#), [3](#), [4](#), [5](#)
- [50] Zhibo Yang, Sounak Mondal, Seoyoung Ahn, Ruoyu Xue, Gregory Zelinsky, Minh Hoai, and Dimitris Samaras. Unifying top-down and bottom-up scanpath prediction using transformers. In *The IEEE Conference on Computer Vision and Pattern Recognition (CVPR)*, 2024. [2](#)
- [51] Zhibo Yang, Sounak Mondal, Seoyoung Ahn, Ruoyu Xue, Gregory Zelinsky, Minh Hoai, and Dimitris Samaras. Unifying top-down and bottom-up scanpath prediction using transformers. In *Proceedings of the IEEE/CVF Conference on Computer Vision and Pattern Recognition*, pages 1683–1693, 2024. [10](#)
- [52] Yuan Yao, Tianyu Yu, Ao Zhang, Chongyi Wang, Junbo Cui, Hongji Zhu, Tianchi Cai, Haoyu Li, Weilin Zhao, Zhihui He, et al. Minicpm-v: A gpt-4v level mllm on your phone. *arXiv preprint arXiv:2408.01800*, 2024. [5](#)
- [53] Jiabo Ye, Haiyang Xu, Haowei Liu, Anwen Hu, Ming Yan, Qi Qian, Ji Zhang, Fei Huang, and Jingren Zhou. mplug-owl3: Towards long image-sequence understanding in multi-modal large language models. *arXiv preprint arXiv:2408.04840*, 2024. [5](#)
- [54] Aohan Zeng, Xiao Liu, Zhengxiao Du, Zihan Wang, Hanyu Lai, Ming Ding, Zhuoyi Yang, Yifan Xu, Wendi Zheng, Xiao Xia, Weng Lam Tam, Zixuan Ma, Yufei Xue, Jidong Zhai, Wenguang Chen, P. Zhang, Yuxiao Dong, and Jie Tang. Glm-130b: An open bilingual pre-trained model. In *ICLR*, 2022. [10](#)
- [55] Jianming Zhang, Shugao Ma, Mehrnoosh Sameki, Stan Sclaroff, Margrit Betke, Zhe Lin, Xiaohui Shen, Brian Price, and Radomir Mech. Salient object subitizing. In *Proceedings of the IEEE Conference on Computer Vision and Pattern Recognition*, pages 4045–4054, 2015. [1](#)
- [56] Tao Zhou, Deng-Ping Fan, Ming-Ming Cheng, Jianbing Shen, and Ling Shao. Rgb-d salient object detection: A survey. *Computational Visual Media*, 7:37–69, 2021. [8](#)
- [57] Deyao Zhu, Jun Chen, Xiaoqian Shen, Xiang Li, and Mohamed Elhoseiny. Minigt-4: Enhancing vision-language understanding with advanced large language models. *ArXiv*, abs/2304.10592, 2023. [10](#)

Models	Prominence			Subtitizing			Prioritizing			Free-viewing			Searching					
	Overall Acc \uparrow	Q1 Acc \uparrow	Q2 Acc \uparrow	Q2 MAE \downarrow	Q2 RMSE \downarrow	Q3 Acc \uparrow	Q4 Acc \uparrow	Q5 Acc \uparrow	Q6 Acc \uparrow	Q7 Acc \uparrow	Q8 Acc \uparrow	Q9 M-Dir \uparrow	Q9 M-Pos \uparrow	Q10 Acc \uparrow	Q11 Acc \uparrow	Q12 M-Dir \uparrow	Q12 M-Pos \uparrow	Q13 Acc \uparrow
Random guess	0.2806	0.1994	-	-	-	0.0415	0.5	0.5	0.33	0.33	0.5	-	-	0.25	0.5	-	-	0.25
Proprietary MLLMs																		
GPT4-o	0.3946	0.3139	0.4512	1.3445	3.2614	0.0924	0.6112	0.6260	0.3399	0.4725	0.5210	0.5917	0.8042	0.2368	0.5514	0.5106	0.7834	0.2731
GPT5-nano	0.4435	0.4664	0.4931	1.1840	2.2897	0.1039	0.6625	0.7177	0.4352	0.4803	0.5743	0.5961	0.8143	0.2264	0.7946	0.4884	0.8004	0.4120
GPT5-mini	0.4675	0.4896	0.5493	1.0080	2.0429	0.1270	0.7025	0.6613	0.4095	0.4835	0.5829	0.6088	0.8100	0.2241	0.8432	0.6150	0.8394	0.4861
Gemini-1.5-Flash	0.3886	0.3323	0.5106	1.3070	3.0978	0.0427	0.5375	0.6855	0.3435	0.4560	0.5297	0.6128	0.8392	0.2417	0.5297	0.5199	0.8206	0.2963
Gemini-2.0-flash	0.4754	0.5189	0.5308	1.1501	2.5422	0.1490	0.7100	0.6935	0.4523	0.4714	0.5804	0.6251	0.8396	0.2483	0.8054	0.6378	0.8583	0.3889
Gemini-2.0-flash-lite	0.3556	0.3932	0.3208	2.0530	4.4785	0.0704	0.6288	0.6532	0.2983	0.4725	0.5223	0.6085	0.7996	0.2437	0.4973	0.5411	0.8170	0.3009
Gemini-2.5-flash	0.4221	0.4408	0.3865	2.2709	5.9720	0.1397	0.6750	0.7258	0.4034	0.5220	0.6176	0.6298	0.8393	0.2253	0.8054	0.6252	0.8540	0.4028
Gemini-2.5-flash-no-thinking	0.4148	0.4774	0.4321	2.0069	4.9635	0.1120	0.6800	0.6694	0.3888	0.5000	0.5532	0.6165	0.8481	0.2149	0.5459	0.5221	0.8202	0.3148
Gemini-2.5-flash-lite	0.4071	0.4457	0.4608	1.3977	4.1724	0.0716	0.6413	0.6855	0.3423	0.5385	0.5260	0.5640	0.8460	0.2667	0.4865	0.4693	0.8361	0.2963
Gemini-2.5-pro	0.4754	0.5189	0.5308	1.1501	2.5422	0.1490	0.7100	0.6935	0.4523	0.5714	0.5804	0.6251	0.8396	0.2483	0.8054	0.6378	0.8583	0.3889
OpenSource MLLMs																		
DeepSeek-VL	0.3655	0.3223	0.4544	1.2471	2.2514	0.0000	0.5750	0.6423	0.3667	0.4890	0.5149	0.5118	0.5450	0.1862	0.5514	0.4790	0.7130	0.1806
Idefics2	0.3067	0.2015	0.2990	2.2078	3.8573	0.0069	0.4950	0.6210	0.3301	0.4396	0.4926	0.5151	0.5525	0.2440	0.5297	0.5322	0.7619	0.2639
Idefics3	0.3552	0.2149	0.4852	1.1055	1.9567	0.0035	0.5625	0.5323	0.3839	0.4396	0.5062	0.5329	0.6310	0.1876	0.4541	0.5407	0.6856	0.1389
LLaVA-Next	0.3460	0.3223	0.3961	1.3727	2.2675	0.0242	0.6000	0.6048	0.3460	0.4011	0.5025	0.5249	0.5998	0.1646	0.5351	0.5083	0.7883	0.1343
LLaVA-OneVision	0.4035	0.4640	0.4517	1.1206	1.9671	0.0381	0.6737	0.5806	0.3362	0.3077	0.5099	0.5490	0.8177	0.2762	0.6432	0.5047	0.7295	0.3611
mPLUG-Owl3	0.3076	0.3309	0.2688	2.8941	4.6162	0.0000	0.6100	0.5565	0.3521	0.4231	0.4418	0.5028	0.4941	0.1908	0.4595	0.5368	0.5592	0.1019
MiniCPM-V 2.6	0.3476	0.3748	0.4491	1.2471	2.1137	0.0370	0.4812	0.6129	0.3447	0.3242	0.4728	0.5132	0.5589	0.1438	0.4757	0.4953	0.7107	0.2269
ERNIE-4.5-VL-28B-A3B	0.3936	0.4115	0.4496	1.5673	3.7682	0.0878	0.6012	0.6210	0.3582	0.4231	0.5124	0.5562	0.8495	0.2506	0.5297	0.5120	0.7913	0.2870
InternVL2.0	0.3082	0.3101	0.3405	2.3458	3.6068	0.0473	0.5738	0.5806	0.3472	0.5165	0.4715	0.5028	0.7090	0.2195	0.4378	0.5016	0.7282	0.1759
InternVL3.5-8B	0.4254	0.4811	0.5111	1.1426	2.1146	0.0543	0.6837	0.6935	0.3741	0.4670	0.5136	0.5013	0.6447	0.2103	0.7081	0.4683	0.7919	0.2963
GLM-4.1V-9B-Base	0.3932	0.4664	0.4040	1.3828	2.3392	0.0693	0.6363	0.6290	0.4401	0.5385	0.5248	0.5139	0.7772	0.1828	0.5838	0.4976	0.7625	0.1759
GLM-4.1V-9B-Thinking	0.4208	0.4908	0.3828	1.9014	3.5067	0.0843	0.6800	0.6048	0.4230	0.5055	0.5916	0.5964	0.7849	0.2770	0.7243	0.5239	0.8353	0.3704
GLM-4.5V	0.4640	0.4737	0.5286	1.2582	2.6779	0.1270	0.6963	0.6613	0.4597	0.5330	0.5421	0.5982	0.7756	0.2678	0.7676	0.5343	0.8096	0.4352
Qwen2-VL-8B	0.4076	0.4103	0.5090	1.4698	2.6747	0.0589	0.6687	0.6016	0.4389	0.3791	0.5718	0.5199	0.7178	0.0828	0.6919	0.4610	0.8200	0.1898
Qwen3-VL-8B	0.4320	0.4811	0.4539	1.1363	1.9546	0.0912	0.6812	0.6371	0.4315	0.4670	0.5507	0.5122	0.8421	0.2621	0.6378	0.4812	0.8613	0.4167
Qwen3-VL-235B-A22B	0.4851	0.5092	0.5223	1.0483	1.9148	0.1305	0.6875	0.6774	0.4291	0.4121	0.7562	0.5665	0.8468	0.2724	0.8703	0.5109	0.8517	0.4167

Table 11. **HVSBench Leaderboard.** The results of leading MLLMs reveal significant room for improvement.

Baselines	# Param	PO \uparrow	SU \uparrow	PI \uparrow	FV \uparrow	SE \uparrow
GPT4-o mini [1]	N/A	0.3126	0.4480	0.3312	0.3560	0.3766
GPT4-o [1]	N/A	0.3139	0.4512	0.3621	0.3737	0.4015
DeepSeek-VL [31]	1.3B	0.1758	0.2513	0.2950	0.3188	0.2843
	7B	0.3223	0.4544	0.3327	0.3445	0.3516
Qwen2-VL [47]	2B	0.0220	0.3499	0.1100	0.2439	0.2643
	7B	0.4103	0.5090	0.3901	0.3182	0.4214
	72B	0.4957	0.4889	0.4158	0.4299	0.5810

Table 12. **Ablation study of The number of params.** PO, SU, PI, FV and SE means “Prominence”, “Subitizing”, “Prioritizing”, “Free-viewing”, “Searching”, respectively.